Improved Atmospheric Density Estimation and Characterization of Uncertainty

By

Alex Sizemore

B.Sc., The University of Kansas, 2014

Submitted to the graduate degree program in Aerospace Engineering and the Graduate Faculty of the University of Kansas in partial fulfillment of the requirements for the degree of Doctor of Philosophy.

Chair: Dr. Craig A. McLaughlin

Dr. Thomas Cravens

Dr. Mark Ewing

Dr. Saeed Farokhi

Dr. Shawn Keshmiri

Date Defended: 30 August 2018

The dissertation committee for Alex Sizemore certifies that this is the approved version of the following dissertation:

Improved Atmospheric Density Estimation and Characterization of Uncertainty

Chair: Dr. Craig A. McLaughlin

Date Approved: 31 August 2018

ABSTRACT

Precise knowledge of the density in the upper atmosphere is a vital component of the orbit determination process for low Earth orbit, as inaccuracies in the estimation of atmospheric drag are the primary source of uncertainty for satellites in low Earth orbit. The need for a more accurate knowledge of the density of the upper atmosphere has led to the development of atmospheric density derived from precision satellite orbits. This method, using the Precise Orbit Ephemerides (POE) for a satellite, requires refinement and validation before it can be used on a larger scale. Additionally, the uncertainty of this method is not well documented.

To improve these atmospheric density models, the POE densities are calculated and compared to the accelerometer derived densities for a majority of the lifetime of both the Challenging Minisatellite Payload (CHAMP) and Gravity Recovery and Climate Experiment (GRACE) satellites to provide a more robust understanding of the effectiveness of these models. Additionally, the framework has been set so that future satellite missions can easily be ingested and analyzed without a substantial amount of work.

In a few locations in the accelerometer derived densities, there are gaps that must be filled. By using a separate accelerometer density method, the first, more reliable accelerometer method can be patched in these locations to allow for a much more robust method. This combined density allows for a more effective evaluation of the POE densities.

To further improve the estimates of atmospheric density, the four Atmospheric Neutral Density Experiment (ANDE) satellites are considered. These spherical satellites provide a much simpler analysis of the atmospheric drag than the much more complicated geometry of the established CHAMP and GRACE satellites. To further improve the estimates for the ANDE satellites, a series of methods to more accurately model the drag coefficients for these satellites are studied and applied to the orbit determination process. In addition to the ANDE satellites, the CHAMP and GRACE satellites drag coefficients were updated to include a higher fidelity drag coefficient and projected area model.

Using these drag coefficients, the atmospheric densities are estimated, and the uncertainty associated with the estimation process is saved. The returned atmospheric densities for the CHAMP and GRACE satellites show a marked improvement in the RMS values when compared to the accelerometer derived densities. Next, a method of validating the ANDE results is examined.

By examining both the uncertainty in the atmospheric density estimate and the error as compared to the accelerometer derived densities for both the CHAMP and GRACE satellites, a scale factor relating these two variables is studied. This method provides a daily scale factor to adjust the uncertainties in the atmospheric density estimate to determine the root mean square (RMS) error for the ANDE satellites. These RMS values are then separated into several geomagnetic and solar activity bins that allow for a better comparison of the results. From this, the effectiveness of the atmospheric density estimation process is evaluated, and the most effective drag coefficient method is selected.

In conclusion, three distinct advancements have been made. First, the drag coefficients have been determined for the ANDE satellites using a larger set of separate methods than have previously been studied, including the Cercignani-Lampis-Lord with a series of separate adsorption models. Second, the POE method is altered to allow for these drag coefficients to be used directly instead of estimated. Finally, by investigating the difference in the uncertainties of the CHAMP and GRACE satellites with their RMS errors, an estimate of RMS errors for a satellite without a base truth model are provided for the first time.

ACKNOWLEDGEMENTS

I would like to thank Dr. McLaughlin for the opportunity and privilege of working on this topic, and his insight and assistance provided for my entire time as a graduate student here at the University of Kansas. His assistance was vital in keeping me on the right track and illuminating new and interesting topics. I would like to thank Doctors Cravens, Ewing, Farokhi, and Keshmiri for sitting on my dissertation committee. Additionally, I would like to extend my thanks to the entire Aerospace Engineering department for everything they have done for me. I would not be where I am today without the outstanding professors and staff that work in this department.

This research was made possible through the help of several different parties. Academic funding was provided in part by the 2018 Summer Research Scholarship from the University Of Kansas Office Of Graduate Studies. Additional funding was provided by the Department of Aerospace Engineering through graduate teaching assistant positions. To Doctors Ewing, Hale, and McLaughlin I am especially grateful for the opportunity to work with you and learn to instruct students in a collegiate environment. Without your assistance in securing funding, none of this would have been possible. Additionally, I would like to thank Dr. Piyush Mehta for his assistance, especially on the drag coefficient sections of this dissertation. Your input and assistance were vital to the completion of this work.

To Iris, who has been there for everything for the past two years, thank you for the moral support throughout the long hours of writing. Finally, I would like to thank my family for their support throughout this process. Their continued support throughout my journey at the University of Kansas has been necessary, and I could not have done it without them.

TABLE OF CONTENTS

NOMENCLATURE

Latin Symbol	Description	Units
A	Area	m^2
A	Freundlich Isotherm Constant	~
a_{drag}	Acceleration Due to Drag	m/s^2
B	Temkin Isotherm Constant	~
C_d	Drag Coefficient	~
d	Particle Diameter	m
H	Scale Height	km
K	Langmuir Isotherm Constant	~
k_b	Boltzmann Constant	J/K
Kn	Knudsen Number	~
L	Knudsen Number Representative Length	m
M	Molecular Mass	u
m	Mass	kg
N	Number of Values	~
n	Number Density	~
P_O	Partial Pressure of Atomic Oxygen	Pa
s	Speed Ratio	~
t	Time	s
T_∞	Ambient Temperature	K
T_s	Surface Temperature	K
U	Satellite Speed	m/s

v ..... Velocity ..... m/s

v_{mp} ..... Most Probable Velocity ..... m/s

x ..... Data Set ..... ~

$\bar{x}$ ..... Mean Value ..... ~

y ..... Truth Data Set ..... ~

$\bar{y}$ ..... Truth Mean Value ..... ~

z ..... Altitude ..... km

Greek Symbol ..... **Description** ..... **Units**

α ..... Accommodation Coefficient ..... ~

β ..... CLL Model Scaling Parameter ..... ~

γ ..... CLL Model Scaling Parameter ..... ~

δ ..... CLL Model Scaling Parameter ..... ~

ζ ..... CLL Model Scaling Parameter ..... ~

η ..... Temkin Isotherm Constant ..... ~

θ ..... Angle ..... deg, rad

θ ..... Percentage of Satellite Coverage ..... %

μ ..... Mass Ratio ..... ~

ξ ..... Freundlich Isotherm Constant ..... ~

$\tilde{\rho}$ ..... Density Error ..... kg/m^3

ρ ..... Density ..... kg/m^3

Abbreviation/Acronym	**Definition**
ANDE	Atmospheric Neutral Density Experiment
ANDE-RR	Atmospheric Neutral Density Experiment – Risk Reduction
BC	Ballistic Coefficient
CC	Cross Correlation
CHAMP	Challenging Mini-satellite Payload
CIRA	COSPAR International Reference Atmosphere
CLL	Cercignani-Lampis-Lord
COSPAR	Committee on Space Research
CPF	Consolidated Prediction Format
CRD	Consolidated Laser Ranging Data
DRIA	Diffuse Reflection with Incomplete Accommodation
EUV	Extreme Ultraviolet
FCal	Fence Calibration
GITM	Global Ionosphere Thermosphere Model
GPS	Global Positioning System
GRACE	Gravity Recovery and Climate Experiment
GSI	Gas-Surface Interaction
HASDM	High Accuracy Satellite Drag Model
ILRS	International Laser Ranging Service
MAA	Mock ANDE Active
MSISE	Mass Spectrometer Incoherent Scatter Extension
NRLMSISE	Naval Research Lab Mass Spectrometer Incoherent Scatter Extension

ODTK ..... Orbit Determination Tool Kit

POE ..... Precise Orbit Ephemerides

RMS ..... Root Mean Square

RSO ..... Rapid Science Orbit

SLR ..... Satellite Laser Ranging

STAR ..... Space Three-axis Accelerometer for Research

LIST OF FIGURES

LIST OF TABLES

1 INTRODUCTION

1.1 Objective

The two primary objectives of the research presented in this dissertation are to quantify and reduce the inherent uncertainty involved in the estimation of atmospheric density model corrections. To complete the first objective, this uncertainty must be determined. This is a fundamental portion of the orbit determination process but has not been closely examined in previous work. Once this first task is completed, higher accuracy models of the inputs to the estimation process, namely the area and drag coefficient, have been incorporated into the results to reduce the uncertainty. These two objectives aim to provide a much richer understanding of the uncertainty involved with the estimation of the density in Earth's upper atmosphere.

1.2 Motivation

The density of the upper atmosphere is one of the largest sources of uncertainty in orbit determination for low Earth orbiting satellites. This uncertainty leads to a poor understanding of the atmospheric drag encountered by these satellites. An accurate model of atmospheric density is important for all operators of these artificial satellites. Having an accurate knowledge of the atmospheric effects on a satellite can be used to predict its life-span, allowing for more accurate prediction of reentry times and locations, and can even prevent satellite collisions.

This requirement of an accurate atmospheric density prediction model has led to the development of many different atmospheric models, several of which can be found below in Figure 1.1 [1] .

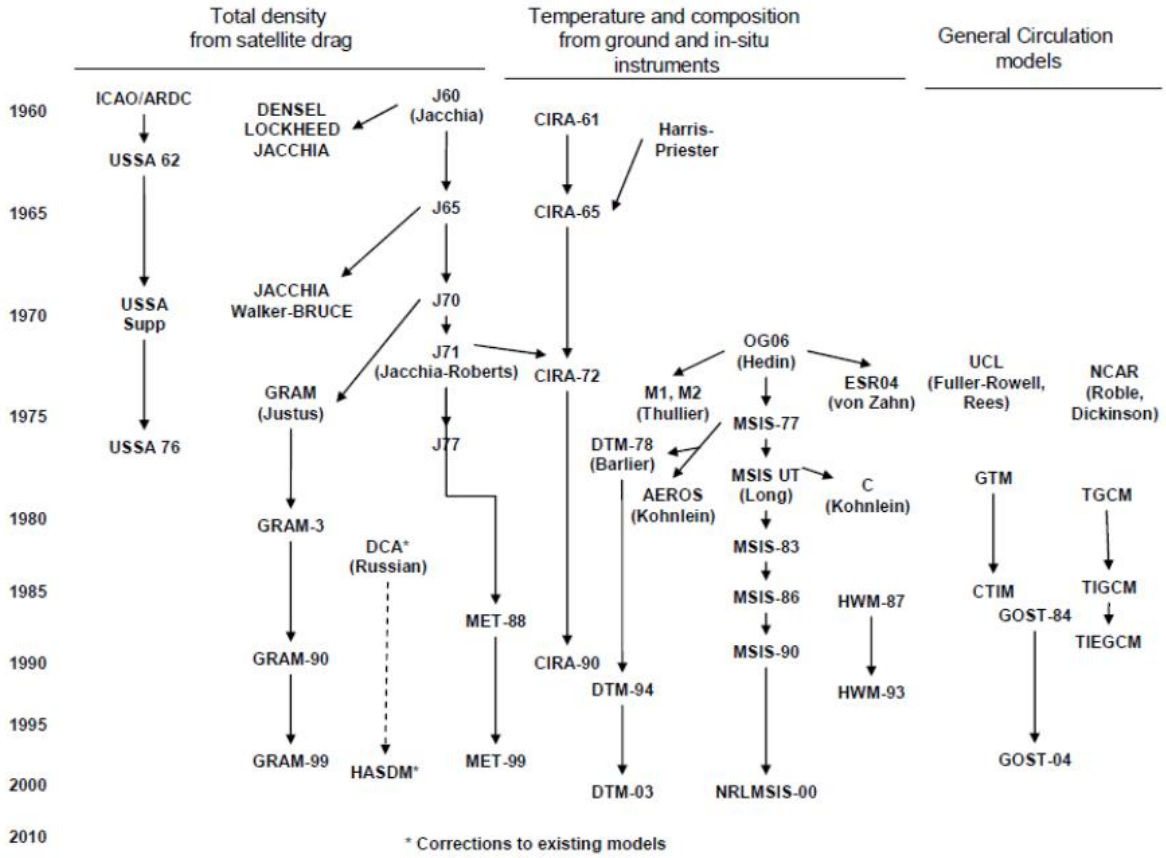

Figure 1.1: Development of Atmospheric Models [1]

As can be seen in the above figure, many of these atmospheric models stem from measurements taken by satellite missions. However, these measurements generally require a dedicated instrument, such as an accelerometer or a mass-spectrometer to analyze the atmosphere. A method that does not require dedicated instrumentation, but instead is derived directly from the dynamics of the satellite can be a very valuable addition to the atmospheric modelling process.

The Precise Orbit Ephemerides (POE) method studied by McLaughlin et. al [2], which is further discussed in Section 1.3, utilizes this method. At present, the uncertainty of the atmospheric density corrections has not been deeply studied. There is a need to quantify the uncertainty associated with these derived density corrections, which will be necessary to

incorporate them into a novel atmospheric density model, as well as validate them for satellites in which there is no other instrument that can provide atmospheric information.

Utilizing these atmospheric density corrections, along with their associated uncertainties, one can begin to incorporate this method of determining the atmospheric density into existing atmospheric models. One such example of this is the POE Assimilated Global Ionosphere Thermosphere Model (GITM) created jointly by Los Alamos and The University of Kansas as presented in McLaughlin et. al. [3]. The use of these atmospheric densities and their associated uncertainties to develop new atmospheric models will help to improve the understanding of the space environment and ensure that the ever-increasing set of Earth-orbiting satellites can continue to operate safely.

1.3 Description of Precise Orbit Ephemerides (POE) Derived Densities

The POE derived densities are calculated using optimal orbit determination. A sequential measurement processing and filtering scheme is completed with POE data provided for the satellite of interest used as the measurements. The filter estimates a state vector including the position, velocity, atmospheric density, and ballistic coefficient. Smoothing is then applied to the result. By considering all data in each solution, the accuracy is increased. The filter/smoother combination can estimate time variable density and ballistic coefficient and includes realistic covariance matrices based on the physics of the problem. [2]

The density is estimated using the method outlined in Wright [4, 5], which is imbedded in the software package Orbit Determination Tool Kit (ODTK). These techniques are considered most useful, as this method allows for a real-time estimation of atmospheric density, as well as

the ballistic coefficient. This is important, as the ballistic coefficient is not well known for all satellites examined.

The estimated atmospheric densities are given as a correction to an existing atmospheric model. These corrections can be applied to Jacchia 1971 [6], Jacchia-Roberts [7], Jacchia-Bowman 2008 [8], COSPAR International Reference Atmosphere (CIRA) 1972 [9], Mass Spectrometer and Ground-Based Incoherent Scatter Extended (MSISE)-1990 [10], or Naval Research Lab MSISE (NRLMSISE)-2000 [11] models. At present, the CIRA-72 model is used as the baseline, as it provides the results that correlate most closely to the accelerometer densities according to Mysore Krishna [12].

1.4 Description of Accelerometer Densities

The accelerometer derived densities, provided by Sutton [13] and Bruinsma [14] are used as the truth values for all error metrics used to validate the performance of the POE derived densities. An additional set of accelerometer densities are derived from the work of Sutton using adjusted drag coefficients and projected areas by Mehta et. al. [15]. These sets of accelerometer data are used to determine the performance of the data after adding these values. The specific error metrics are explained in Section 2.1. To determine the true atmospheric density experienced by a satellite, accelerometer data collected from the Challenging Mini-satellite Payload (CHAMP) and the Gravity Recovery and Climate Experiment (GRACE) satellites were used.

Prior to using the accelerometer data, however, the measurements must be preprocessed. First, spikes in the accelerometer data caused by station keeping maneuvers and parasite electric currents are removed. Second, the data is smoothed with a low-pass filter and data gaps are filled

with interpolation. Finally, the data is validated and calibrated by applying instrumental biases and scale factors.

Once this is completed, all factors not related to atmospheric drag must be eliminated. Solar radiation pressure, as well as Earth albedo must be accounted for. Once these perturbations are removed, the drag signal remains. Finally, the atmospheric density is found by applying the following equation:

$$\boldsymbol{\rho = \frac{2a_{drag}m}{C_dAv^2}} \quad \textbf{(}\text{Eq. 1.1)}$$

where ρ is the atmospheric density, a_{drag} is the acceleration captured by the previous procedure, m is the mass of the satellite, C_d is the drag coefficient of the satellite, A is the area normal to the flow past the satellite, and v is the scalar velocity of the satellite relative to the atmosphere. Each of the parameters on the right-hand side of the equation is assumed to be known.

1.5 Description of Methods to Determine Drag Coefficients

As discussed in the previous section, when one is determining atmospheric density, a precise and accurate knowledge of all parameters that go into the calculation of the drag force on a satellite is necessary. The mass of a satellite is known from the time of launch and is well estimated as it continues throughout its life. The area of the satellite normal to the flow is well known and constant for a spherical satellite; and can be easily calculated given knowledge of orientation in the case of a non-spherical satellite. The dynamics of the satellite, such as its velocity must be well known as a prerequisite for the estimation of the density. The drag coefficient is generally the primary source of uncertainty, after atmospheric density, when considering the drag on a satellite.

Previously, in the work done by McLaughlin et. al. [16], the ballistic coefficient, and indirectly the coefficient of drag are estimated along with the atmospheric density using a Gauss-Markov process. This procedure has provided an effective estimate of the ballistic coefficient and atmospheric density simultaneously; however, the estimated density and nominal ballistic coefficient are coupled. A bias in the nominal ballistic coefficient results in a bias in the estimated atmospheric density. As a result, there is a need for a more direct knowledge of the drag coefficient.

Determination of the drag coefficient for a satellite is a uniquely difficult situation in the space environment. This drag coefficient is heavily dependent on the gas-surface interaction (GSI) between the satellite and its surrounding environment. Figure 1.2 [17] below illustrates several assumptions of gas-surface interactions.

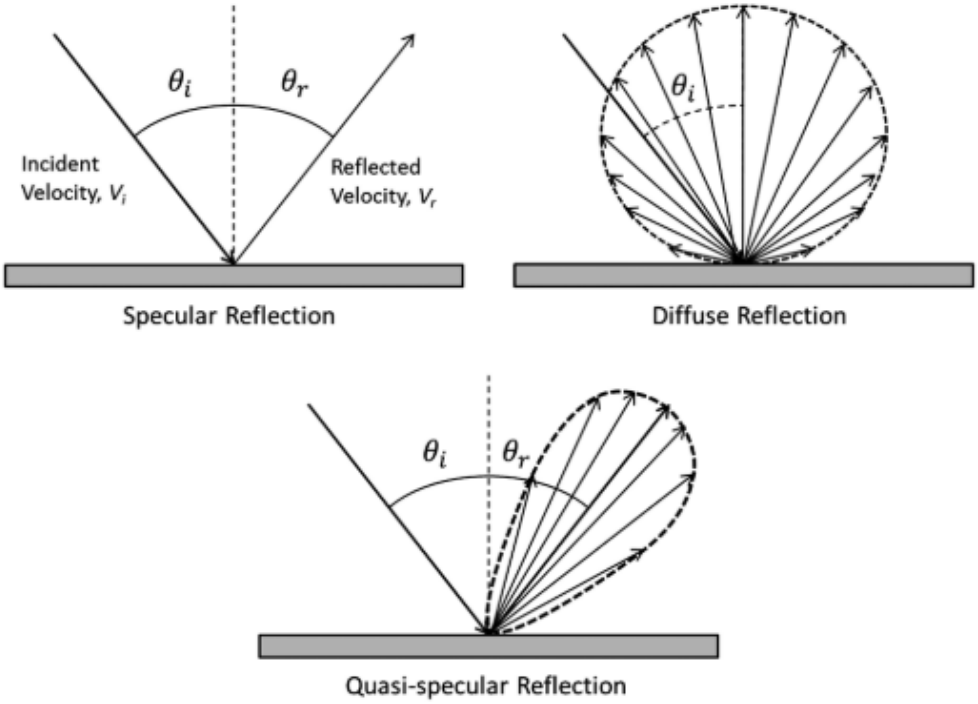

Figure 1.2: Representation of Gas-Surface Interaction Models [17]

Assuming diffuse reflection of particles, Moe et. al. [18] discusses realistic drag coefficients to use for a series of satellite geometries, specifically spherical, conical, cylindrical, and flat plate modeled satellites. Included in this article is a series of tables for accommodation coefficients of 1.00, 0.95, and 0.90; surface temperatures of 500-1500 kelvin in 500 K increments; and mean molecular mass of atmospheric particles of 18 and 22. Through interpolation, the drag coefficients for any value contained within these ranges can be calculated with a reported uncertainty of 4%. Additional work completed by Moe et. al. [19] provides a deeper investigation for a spherical satellite. In this work, the drag coefficient is plotted with respect to altitude using both diffuse and quasi-specular reflections.

Pilinski et. al. [20] created a model that fits drag coefficient data found in Bowman and Moe [21] to a Langmuir isotherm [22]. This model used the NRLMSISE-00 model discussed in Section 1.7.2 to determine the number density of atomic oxygen and atmospheric temperature as inputs to the isotherm. This accommodation model is valid for altitudes below 500 km, and accommodation coefficients greater than 0.85.

Mehta et. al. [17] discusses two GSI models that can be used to determine the time varying drag coefficient given the surrounding environment: the quasi-specular Cercignani-Lampis-Lord (CLL) [23], and the diffuse reflection with incomplete accommodation (DRIA) [20] models. These models have several parameters that must be estimated prior to their use. Several of the constant parameters and their range of validity are discussed in Walker et. al. [24] In addition to several tuning constants, knowledge of the amount of atomic oxygen on the surface of the satellite is required. These values are modeled by a series of adsorption models: the Langmuir isotherm

[22], the Freundlich isotherm [25], and the Temkin isotherm [26]. Each of these values are then used to calculate the adsorption constant and plugged into the two GSI models.

For the non-spherical satellites studied, the drag coefficient is not the only variable parameter that must be known. In these cases, one must also know the area normal to the incoming flow. In these cases, the orientation of the satellite must also be known. For the non-spherical satellites studied, effective areas derived from the satellite's orientation and Langmuir CLL drag coefficients are made available by Mehta et. al. [15] for the CHAMP and GRACE satellites.

1.6 Brief Introduction of Satellite Missions Studied

A summary of the basic parameters of interest for each of the satellites discussed can be found in Table 1.1. For GRACE, the reentry date is not the exact date of reentry of the satellites, but instead the date that was deemed the end of mission for the two satellites. A deeper discussion of each of these satellites can be found in the subsequent sections.

Table 1.1: Satellite Properties

Satellite	Deployment Date	Reentry Date	Cross Sectional Area (m^2)	Mass (kg)	Initial Altitude (km)	Inclination (deg)
CHAMP	July 15, 2000	September 20, 2010	Variable (See Figure)	522	454	87
GRACE-1+2	March 17, 2002	October, 27, 2017*	Variable (See Figure)	432	485	89
ANDE-RR FCal	December 21, 2006	May 25, 2008	0.1551792	62.7	350	51.6
ANDE-RR MAA	December 21, 2006	December 25, 2007	0.1829214	52.04	350	51.6
ANDE-2 Castor	July 30, 2009	August 18, 2010	0.1829214	47.5	350	51.6
ANDE-2 Pollux	July 30, 2009	March 28, 2010	0.1829214	27.4	350	51.6

1.6.1 **Challenging Mini-satellite Payload (CHAMP)**

The Challenging Minisatellite Payload (CHAMP) mission [27] was to study variations in the magnetic and gravity fields of Earth. Figure 1.3 below shows an artist's impression of the CHAMP satellite in flight.

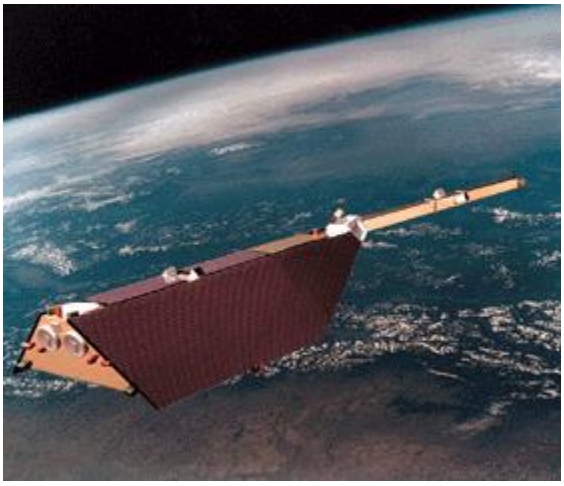

Figure 1.3: Artist Representation of CHAMP Satellite in Flight [27]

The CHAMP satellite was launched from the Plesetsk Cosmodrome July 15, 2000. It orbited the Earth at an 87° inclination at an initial altitude of 454 km. The satellite reentered on September 20, 2010, exceeding its expected lifetime by 5 years. The instruments of interest on this satellite are the retroreflector array for satellite laser ranging (SLR) and the GPS receiver, which allow for high accuracy orbit determination, and the Space Three-axis Accelerometer for Research (STAR) accelerometer, which enables accelerometer derived density comparisons. The initial mass of the satellite was 522kg, 30 kg of which was attributed to the cold gas thrusters, which allowed for three boost maneuvers. Figure 1.4 below illustrates the basic geometry of the CHAMP satellite.

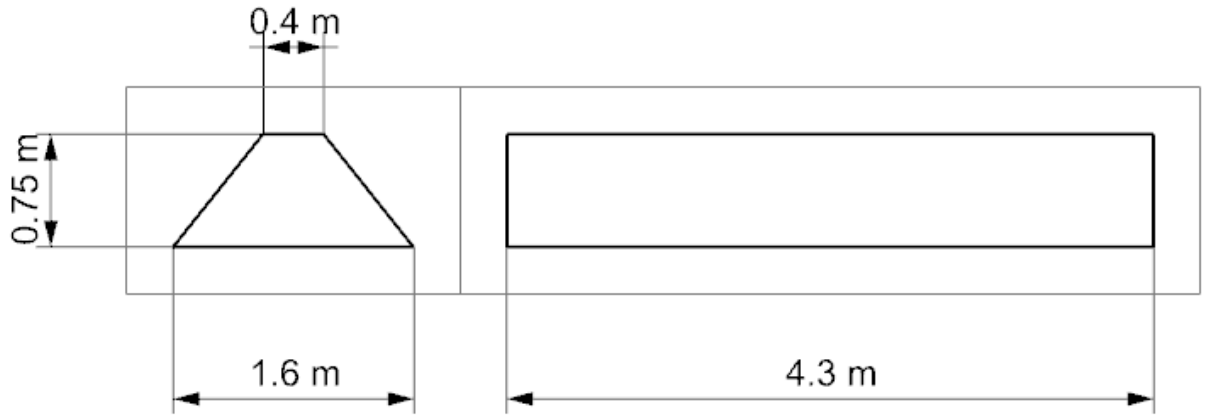

Figure 1.4: CHAMP Satellite Geometry

1.6.2 Gravity Recovery and Climate Experiment (GRACE)

The Gravity Recovery and Climate Experiment (GRACE) mission [28] consisted of two tandem satellites used to detect perturbations in Earth's gravity field to estimate differences in mass distribution. Figure 1.5 below shows an artist's depiction of the two satellites in operation.

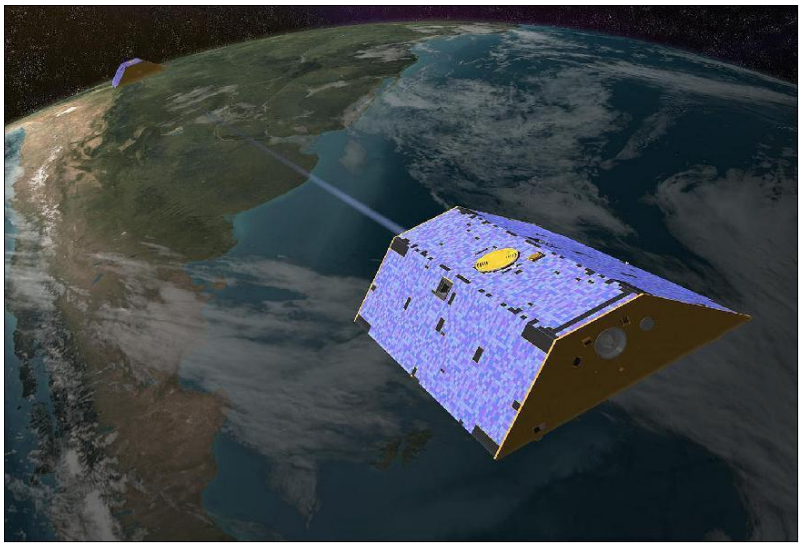

Figure 1.5: Artist Depiction of GRACE Satellites in Orbit [28]

The two satellites were launched from the Plesetsk Cosmodrome on March 17, 2002. The GRACE satellites orbit the Earth at an inclination of 89° and an altitude of 485 km, decaying to 300 km after 5 years. Like CHAMP, the original mission was intended to be 5 years. However, the mission was continued until October 27, 2017, a full 10 years past its intended lifetime. Despite the end of the mission, contact has been lost with only one of the two GRACE satellites. GRACE-B's fuel has been expended, and the satellite has begun to deorbit, expected to return to Earth in December or January. GRACE-A, will use its remaining fuel to "calibrate and characterize its accelerometer", and deorbit in early 2018. A follow-on mission is currently planned to launch in 2018. As with CHAMP, the SuperSTAR accelerometer provided the basis for the accelerometer derived density for comparison purposes. Each of the two GRACE satellites has a mass of 432 kg, with a fuel mass of 34 kg. Figure 1.6 below illustrates the geometry of the GRACE Satellites.

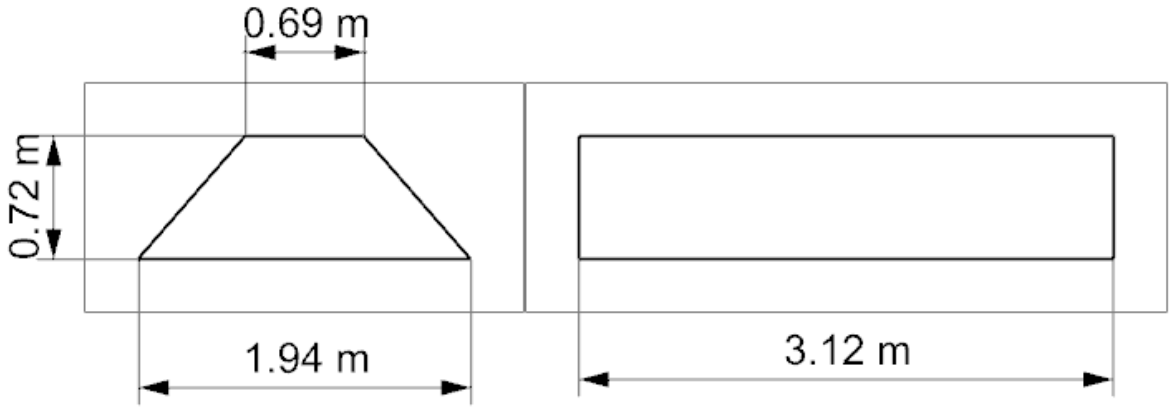

Figure 1.6: GRACE Satellite Geometry

1.6.3 **Atmospheric Neutral Density Experiment Risk Reduction (ANDE-RR)**

The Atmospheric Neutral Density Experiment Risk Reduction (ANDE-RR) flight [29, 30] consisted of two satellites designated Fence Calibration (FCal) and Mock ANDE Active (MAA). Figure 1.7 below shows the two ANDE-RR satellites in their deployment system.

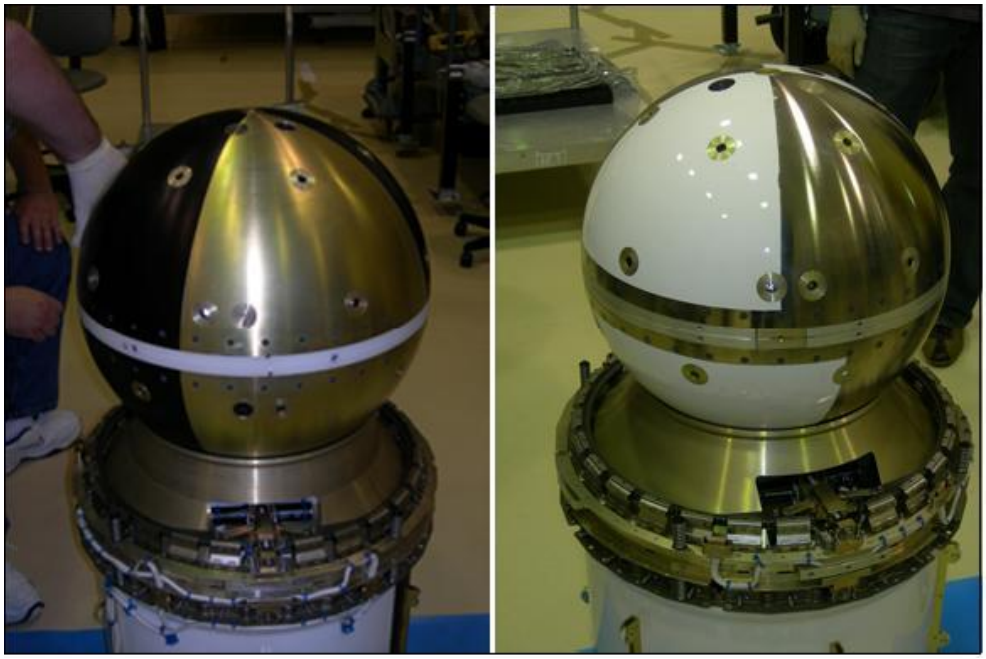

Figure 1.7: ANDE-RR Satellites MAA (left) and FCal (right) [31]

The mission was developed to test the deployment mechanism for the Space Shuttle, as well as the instruments for a future ANDE flight. The risk reduction flight was launched from the Space Shuttle on December 21, 2006. The satellites were fitted with retro-reflectors for SLR and contained a small payload to determine the spin rate and orientation of the spacecraft. The spacecraft masses were 50 and 75 kg for MAA and Fcal, respectively. The satellites were placed in a 350 km orbit at 51.6° inclination. The MAA and FCal satellites re-entered the Earth's atmosphere on December 25, 2007 and May 8, 2008 respectively.

1.6.4 **Atmospheric Neutral Density Experiment 2 (ANDE-2)**

The Atmospheric Neutral Density Experiment 2 (ANDE-2) [32, 33] was a system of two nearly perfectly spherical satellites to monitor atmospheric density. Figure 1.8 below shows the two ANDE-2 satellites prior to launch.

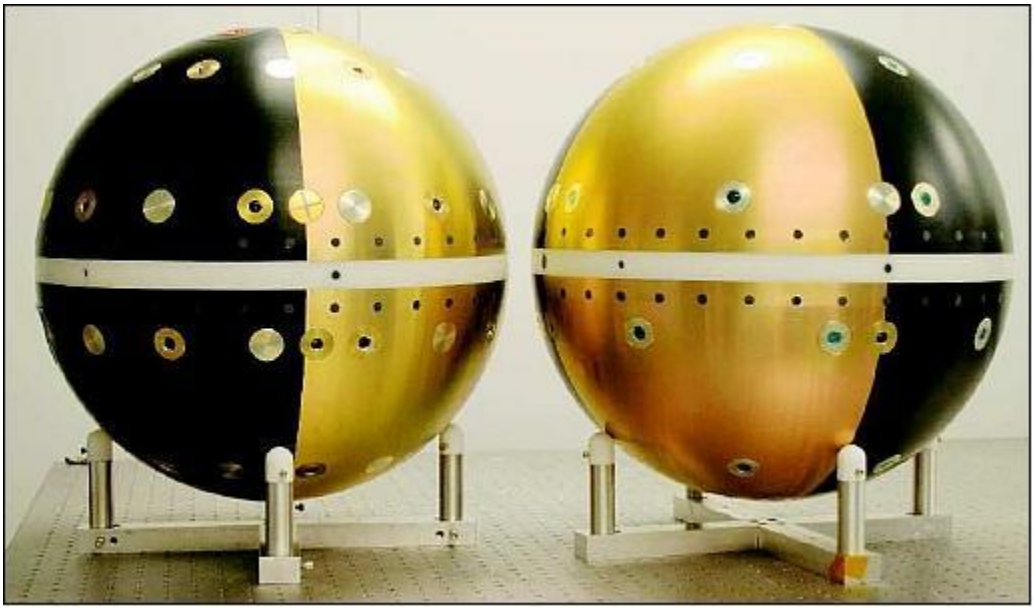

Figure 1.8: ANDE-2 Satellites Castor (left) and Pollux (right) [32]

The two satellites were launched from the Space Shuttle flight STS-127 on July 30, 2009. The system consisted of an active satellite, Castor, and a passive satellite, Pollux. The two satellites were different masses due to the different payloads: Castor with a mass of 47.45 kg, and Pollux with a mass of 27.44 kg. The satellites flew at an altitude of 350 km at an inclination of 51.6°. The ANDE-2 satellites Castor and Pollux re-entered the Earth's atmosphere on August 18 and March 28, 2010 respectively.

1.7 Brief Discussion of Atmospheric Models

1.7.1 COSPAR International Reference Atmosphere – 1972 (CIRA-72)

The COSPAR International Reference Atmosphere-1972 (CIRA-72) [9] model is a combined set of atmospheric models which is valid from 25 km to 2500 km. In the regime in which satellites operate (altitudes > 100 km), the CIRA-72 model is identical to the Jacchia 1971 atmospheric density model on which it is based. The Jacchia 1971 model [6] was developed as a revision of the Jacchia 1970 model, incorporating additional mass spectrometer and EUV-absorption data collected between 1961 and 1969. To account for short-term variations, the models uses an 81-day average for geomagnetic and solar activity levels as inputs.

1.7.2 Naval Research Laboratory Mass Spectrometer and Ground-Based Incoherent Scatter Extended–2000 (NRLMSISE-00)

The Naval Research Laboratory Mass Spectrometer and Ground-Based Incoherent Scatter Extended–2000 (NRLMSISE-00) [11] atmospheric model is an improvement over the earlier MSISE 1990 atmospheric model. The MSISE series of atmospheric models incorporate a large data set of in situ mass spectrometer data collected from Earth orbiting satellites, and incoherent scatter radar data from ground-based locations. The NRLMSISE-00 model incorporates additional satellite drag data using spherical harmonics. The NRLMSISE model requires input of the current and 81-day averages for solar flux measured by the F10.7 parameter, as well as magnetic indices for three-hour intervals up to 9 hours before the current time. The benefit of using the NRLMSISE-00 atmospheric model, however, is that one can obtain the number densities of several species of gases found in the upper atmosphere.

1.7.3 **High Accuracy Satellite Drag Model (HASDM)**

The High Accuracy Satellite Drag Model (HASDM) [34] is an atmospheric model that was developed by the US Air Force to include dynamic changes in atmospheric drag. HASDM includes a dynamic calibration of the atmosphere (DCA) algorithm that incorporates variations in thermospheric density using near real-time observations from a set of low Earth orbit calibration satellites. This atmospheric model pulls inputs of the EUV index, a measure of the extreme ultraviolet radiation. In addition, the model extrapolates data using the last 27 days of measurements through a density prediction filter.

2 METHODOLOGY

2.1 Verification of Established POE Density Metrics

Before any new work can be done to further improve the Precise Orbit Ephemeris (POE) density data, root mean square (RMS) error and cross correlation (CC) between POE and a baseline accelerometer derived density, originally completed by Mysore Krishna, [12] was re-created to ensure that any changes in ODTK software version would not affect the performance of POE with respect to other methods. The method to calculate RMS [35] and CC [36] are found below in Equations 2.1 and 2.2**.**

$$RMS = \sqrt{\sum_{i=1}^{N} \frac{(x_i - y_i)^2}{N}} \quad \text{(Eq. 2.1)}$$

$$\boldsymbol{CC = \frac{\sum_{i=1}^{N}[(x_i - \bar{x})(y_i - \bar{y})]}{\sqrt{\sum_{i=1}^{N}(x_i - \bar{x})^2}\sqrt{\sum_{i=1}^{N}(y_i - \bar{y})^2}}} \quad \text{(Eq. 2.2)}$$

Where x_i and y_i are the ith value of the data set of interest and the truth-values respectively, and $\bar{x}$ and $\bar{y}$ are the mean values of each data set. The results as a comparison to previous work can be found in Section 3.

2.2 Improvements Made to POE Density Metrics

2.2.1 Merging of Sutton and Bruinsma Accelerometer Data

Both the Sutton and Bruinsma accelerometer density data have significant gaps. In several cases, these gaps do not occur in the exact same location. Figure 2.1 and Figure 2.2 below illustrate the gaps in the CHAMP and GRACE data streams respectively.

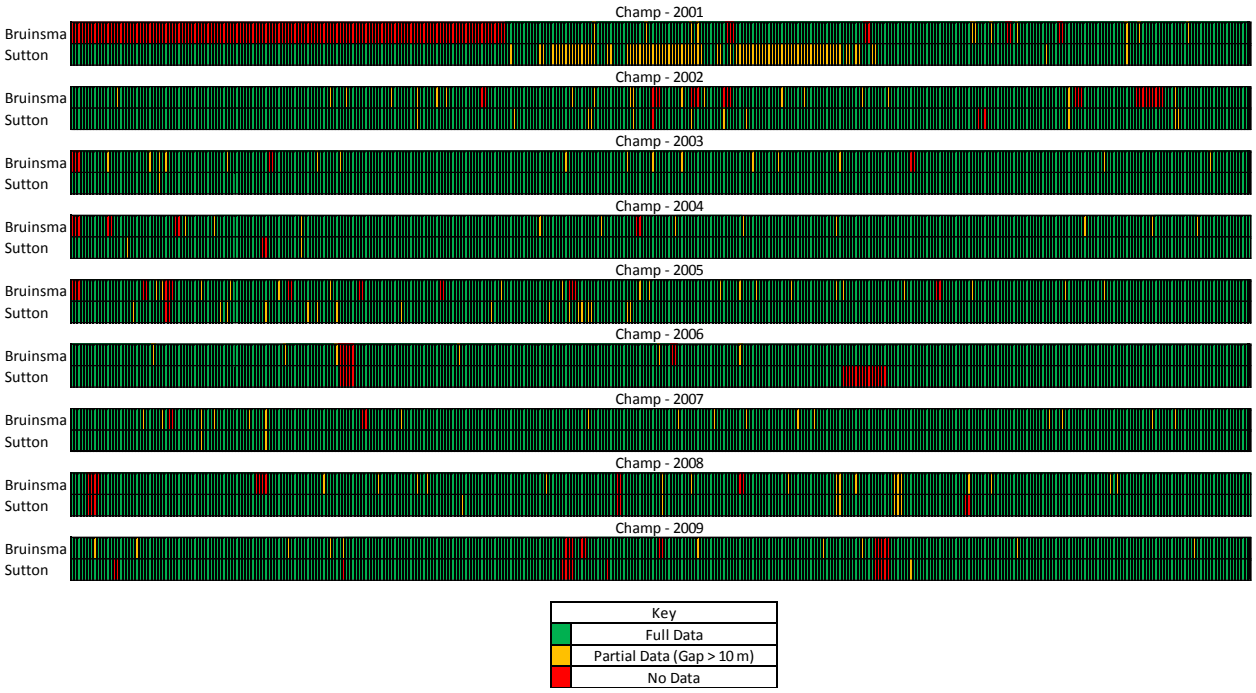

Figure 2.1: Gaps in CHAMP Accelerometer Data

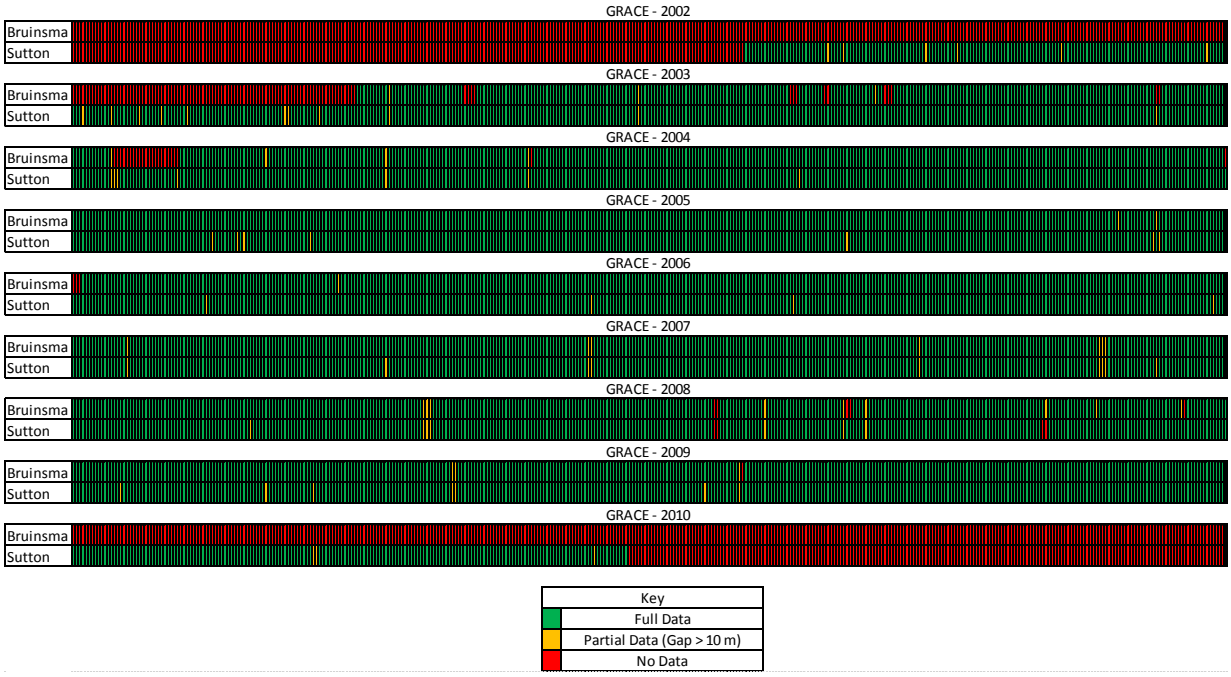

Figure 2.2: Gaps in GRACE Accelerometer Data

These streams of data can be combined in several locations to form one data stream. To complete this process, the Sutton data are used as a baseline, and the Bruinsma data are used to fill in the gaps. Using a linear weighted blending process, a patch of Bruinsma data sized three times larger than the gap in the Sutton data is applied to these locations. However, the Bruinsma data cannot be used to directly patch the Sutton data, as there is a small difference in the values at each point. The Bruinsma data is adjusted for the duration of the patch such that its average value over a time period three times the gap size with an overlap the size of the gap on either side will match the average value of the Sutton data where the patch is applied.

2.2.2 Examination of Cross Correlation and RMS for the Life of a Satellite

Prior work in studying POE focused on calculating the CC and RMS error averaged the CC and RMS errors calculated on a week-by-week basis. However, there are some issues with this procedure. A sounder method of examining these error parameters would be to examine them for

the entire life of the satellite. The results of examining the entire data set instead of the average is explored in Section 4.2.

2.2.3 Absolute Mean Percent Error

In addition to the CC and RMS values that were calculated, a potentially better clarity can be obtained by examining the percent error as opposed to a set value. To accommodate this need, the Absolute Mean Percent Error is calculated using, Equation 2.3 [37] below. These results can be found in Section 4.2.

$$AM\%E = \frac{1}{N}\sum_{i=1}^{N}\frac{|x_i - y_i|}{y_i} \quad \text{(Eq. 2.3)}$$

2.3 Calculation of Drag Coefficients and Normal Areas

First, the altitude, latitude, and longitude, as well as the F10.7 and Ap for a satellite at a given time are fed into the NRLMSISE-00 [11] atmospheric model. This model is used to determine the ambient atmospheric temperature, and the molecular count of Hydrogen, Helium, Oxygen, Nitrogen, Argon atoms, as well as N_2 and O_2 molecules, which are then combined to form the total molar mass of the constituent elements, denoted as M_t.

Next, the most probable speed of a Maxwellian velocity distribution at the local translational temperature is calculated using the following equation:

$$v_{mp} = \sqrt{\frac{2k_bT_\infty}{M}} \quad \text{(Eq. 2.4)}$$

where k_b is the Boltzmann constant, M is the mean molecular mass, and T_∞ is the atmospheric temperature calculated using NRLMSISE-00. This most probable speed is then used to calculate the speed ratio, s, below:

$$s = \frac{v_{rel}}{v_{mp}} \quad \text{(Eq. 2.5)}$$

The second parameter that must be calculated is the energy accommodation coefficient, α. This coefficient is dependent on if the surface of the satellite is covered in atomic oxygen. If the satellite's surface is covered, the value of α is exactly one. However, if the surface of the satellite is clear of atomic oxygen, α is calculated using the empirical model of Goodman and Wachmann [38] as shown below:

$$\alpha = \frac{(2.4\mu)}{(1+\mu)^2} \quad \text{(Eq. 2.6)}$$

where μ is the ratio of the average mass of the atmospheric gas to the particles on the satellite's surface.

Next, the s and α parameters are used to calculate the drag coefficients for both a clean and fully covered satellite according to one of two Gas-Surface Interaction (GSI) models: the quasi-specular Cercignani-Lampis-Lord (CLL) [23] or the Diffuse Reflection with Incomplete Accommodation (DRIA) [20].

The CLL model is given by:

$$C_D = \frac{1}{M_t}\sum_{i=1}^{N} M_i \left(\frac{2+\sqrt{2(1-\alpha)}}{2} \left(\frac{4s^4+4s^2-1}{2s^4}\,\mathrm{erf}(s) + \frac{2s^2+1}{\sqrt{\pi}s^3}\,e^{-s^2} \right) + \frac{2\zeta_i\sqrt{\pi}}{3s^2}\,e^{-\beta_i(2(1-\alpha))^{\gamma_i}} \left(\frac{T_s}{T_\infty}\right)^{0.5+\delta_i} \right)$$

(Eq. 2.7)

where α is the energy accommodation coefficient, M_i and T_∞ are the molar mass of each constituent element and the ambient temperature respectively, as determined using NRLMSISE-00, and erf() is the error function, defined as:

$$\mathrm{erf}(x) = \frac{2}{\sqrt{\pi}}\int_0^x e^{-t^2}dt \qquad \text{(Eq. 2.8)}$$

In addition to these values, the surface temperature of the satellite, denoted as T_s is required. The satellite surface temperature has been shown in Walker et. al. [24] to not have a strong effect on the resultant drag coefficient from 100 to 500 K. As a result, this value is set to be 300 Kelvin for each run, providing a median point to the highest and lowest values found in the previous study.

The other parameters $\beta_i, \gamma_i, \delta_i, and\ \zeta_i$ are functions of the ith species of molecules and free elements contained in the gas. These individual parameters are given below in Table 2.1, and are derived from work completed by Walker et. al. [24].

Table 2.1: Best-Fit Parameters for CLL Drag Equation

Species	β	γ	δ	ζ
O_2	5.45	0.18	0.5	49
N_2	5.5	0.18	0.5	51
O	4.4	0.32	0.48	11
N	4.75	0.24	0.5	20
He	4.15	0.35	0.52	8
H	3.4	0.54	0.54	2.8

The DRIA drag model is given as:

$$C_D = \frac{4s^4+4s^2-1}{2s^4}\text{erf}(s) + \frac{2s^2+1}{\sqrt{\pi}s^3}e^{-s^2} + \frac{2\sqrt{\pi}}{3s}\sqrt{\frac{T_{k,r}}{T_\infty}} \quad \text{(Eq. 2.9)}$$

where $T_{k,r}$ is found by:

$$T_{k,r} = \frac{M_t v_{rel}^2}{3k_b}(1-\alpha) + \alpha T_s \quad \text{(Eq. 2.10)}$$

Since the values of α (and as a result, the drag coefficient) are only known for a fully covered or completely clean satellite surface, we must assume that the drag coefficient of the satellite is some combination of the resultant drag coefficient given a completely clean satellite and a fully covered one. The percentage of the satellite covered is indicated by θ and the remaining percentage of uncovered surface given by $(1-\theta)$. The resulting drag equation is then given by:

$$C_{D_{total}} = (1-\theta)C_{D_{clean}} + \theta C_{D_{covered}} \quad \text{(Eq. 2.11)}$$

To determine the portion of the satellite that is covered, three separate adsorption models are considered: The Langmuir isotherm, the Freundlich model, and the Temkin isotherm. The Langmuir isotherm gives the value of θ as:

$$\theta = \frac{KP_0}{1+KP_0} \quad \text{(Eq. 2.12)}$$

The Freundlich method calculates θ by:

$$\theta = AP_0^{\xi} \quad \text{(Eq. 2.13)}$$

Finally, the Temkin isotherm calculates θ to be:

$$\theta = \frac{1}{B}\ln(\eta P_0) \quad \text{(Eq. 2.14)}$$

In each of these cases, P_0 is the partial pressure of atmospheric oxygen at a given altitude, calculated using the following equation:

$$P_0 = n_o k_b T_\infty \quad \text{(Eq. 2.15)}$$

where n_o is the number density of oxygen obtained from the NRLMSISE-00 model. The other parameters for each of the adsorption models are fitted using optimized values given by Mehta in a discussion on July 10, 2018 are shown below in Table 2.2.

Table 2.2: Best fit of Langmuir, Freundlich, and Temkin adsorption model parameters for the CLL and DRIA GSI models.

Model	Parameter	CLL	DRIA
Langmuir	K	2.89E+06	1.44E+06
Freundlich	A	2.09	3.515
	ξ	0.0708	0.1202
Temkin	B	16.22	10.22
	η	3.36E+11	8.38E+08

In addition to calculating drag coefficients from the two GSI models using the three separate adsorption models, the values for the Langmuir isotherm constants are compared to earlier work completed by Pilinski et. al. [20], which were created using satellite drag coefficients calculated

by Bowman and Moe [21]. This method uses the Langmuir isotherm equation to directly calculate the accommodation coefficient using the following equation:

$$\alpha = \frac{7.50\times10^{-17} n_O T_i}{1+7.50\times10^{-17} n_O T_i} \quad \text{(Eq. 2.16)}$$

This accommodation coefficient is then plugged into the DRIA model to calculate the drag coefficient. Using this procedure, seven separate drag coefficients are generated for each given satellite state. For the CHAMP and GRACE satellites, the Langmuir CLL drag coefficient is not directly calculated, but is found in the appendices of Mehta et. al. [15]

Due to their spherical nature, the ANDE satellites do not have a variable area, and therefore the orientation of the satellite is not required as an input. This is not the case for the non-spherical satellites CHAMP and GRACE. The areas of these satellites normal to the incoming flow are also a data set made freely available in the appendices of Mehta et. al. [15].

Finally, to ensure that during the entire lifetime of the satellite the free molecular flow assumption is held, the Knudsen number is calculated using Equation -0.83 [15] below.

$$Kn = \frac{1}{\sqrt{2}\pi d^2 nL} \quad \text{(Eq. 2.17)}$$

where d is the mean collision diameter, and L is the diameter of the ANDE satellite. If the Knudsen number is larger than 10, the free molecular flow assumption holds [39]. If the Knudsen number is less than 10, the free molecular flow assumption does not hold, and the drag coefficients returned by the model are suspect.

2.4 Orbit Determination and Density Estimation of ANDE Satellites Using Calculated Drag Coefficients

Next, these drag coefficients are used in an orbit determination technique which uses the satellite laser ranging (SLR) data from the ANDE satellites to estimate the atmospheric density encountered by these satellites. This procedure is an expansion on the POE derived density method outlined in McLaughlin et. al. [2], with the main difference being that the ballistic coefficient is not estimated, and is assumed to be a known value imported into the OD technique.

The measurements used in this technique are the Consolidated Laser Ranging Data (CRD) and the Consolidated Prediction Format (CPF), both provided by the International Laser Ranging Service (ILRS) found at ftp://cddis.gsfc.nasa.gov/pub/slr/data/npt_crd/, and ftp://cddis.gsfc.nasa.gov/pub/slr/cpf_predicts/ respectively. The CRD files are converted using ODTK and ingested directly, using an initial sigma of 0.0175 meters, updates using a Gauss-Markov process with a half-life of 15 minutes. The CPF files are converted into a GPS Navsol data file with an uncertainty of 1000 m.

Ideally, the drag coefficients generated in the previous section would then be used as inputs into the orbit determination method to determine the atmospheric density of the satellite. However, ODTK does not allow for the input of a variable coefficient of drag. Instead, a variable area is allowed as an input. ODTK performs the atmospheric density estimation using the ballistic coefficient, calculated as:

$$BC = \frac{m}{C_d A} \qquad \text{(Eq. 2.18)}$$

where A is the area of the satellite, and m is its mass. Since the parameter passed into the filter is the ballistic coefficient, and the only variable parameter allowed by the software is area, we introduce the idea of an "effective area" calculated by:

$$A_{eff} = A_{sat}\left(\frac{C_{d_{acutal}}}{C_{d_{ref}}}\right) \quad \text{(Eq. 2.19)}$$

where A_{sat} is the actual satellite area, given below in Table 2.3 for each satellite, and $C_{d_{ref}}$ is a reference drag coefficient, set to be 2.05.

Table 2.3: Satellite Cross-Sectional Areas for the ANDE Satellites [30, 33]

ANDE-2 Castor	ANDE-2 Pollux	ANDE-RR MAA	ANDE-RR Fcal
0.182921	0.182921	0.182921	0.155179

Once the OD process is set up, an augmented state vector using the atmospheric density and the satellite's state are estimated using a sequential measurement processing and filtering scheme. These filters are run in 4-day segments to ensure that enough SLR data is ingested between runs. After filtering, the data is run through a smoother. This estimated atmospheric density is calculated as a correction to an existing model, with the uncertainty modeled using a Gauss-Markov process. The density correction used a half-life of 180 minutes. For this estimation, the COSPAR International Reference Atmosphere 1972 (CIRA-72) [9] was used as a baseline. This atmospheric model was shown to provide the lowest RMS error in estimation of density in McLaughlin et. al. [2].

2.5 Orbit Determination and Atmospheric Density Estimation for Non-Spherical Satellites

For the CHAMP and GRACE satellites, the atmospheric density is estimated using a similar orbit determination technique as the one outlined in Section 2.4. However, in this case, Rapid

Science Orbits (RSO) have been provided which allow for a direct input of the measured position vector of the satellite as a measurement. As with the ANDE satellites, the ballistic coefficient is not estimated, as the inputs to it are assumed to be well known.

The measurements used in this technique are the previously mentioned RSO, provided by the GFZ-Potsdam, and can be found at https://isdc.gfz-potsdam.de. The RSO files are converted to a GPS style measurement using the Navsol data format, using an uncertainty of 10 meters.

The effective area parameter is then calculated as before. However, one major difference from the previous section is that the area normal to the flow is no longer a constant value. The calculation of the effective area is now the combination of two separate parameters, drag coefficient and area, be folded into a single parameter of effective area. This set of data is then input into the precise orbit determination scheme.

As before, the augmented state vector of the atmospheric density and the satellite's state are estimated using the measurement processing and filtering technique. These filters are run in 14-hour intervals. This is done to allow for some overlap in the resulting files, and to remain compatible with the previously used techniques. The atmospheric density estimation uses the same techniques as the methods used for the ANDE satellites, providing corrections to the CIRA-72 model.

2.6 Determination of Uncertainties

The uncertainty in the atmospheric densities is a by-product of the orbit determination process. The filtering scheme processes the uncertainty in the atmospheric density as a component of the covariance matrix processed by the algorithm. Knowledge of this uncertainty will lead to a better understanding of the errors involved in the density estimation. To evaluate

the capability of these uncertainties to estimate these errors, the atmospheric densities obtained for the CHAMP and GRACE satellites as determined in Section 2.5 are compared to the combined accelerometer densities examined in Section 2.2.1, calculated with updated drag coefficients as seen in Mehta et. al. [15].

The error of the atmospheric estimates was calculated using the accelerometer density found in Mehta et, al. [15] as the truth-value. This error is shown in Equation 2.20 below:

$$\tilde{\rho} = \rho_{e_i} - \rho_{a_i} \qquad \text{(Eq. 2.20)}$$

where $\tilde{\rho}$ is the density error, ρ_{a_i} is the ith accelerometer derived atmospheric density, and ρ_{e_i} is the ith estimated density. The daily RMS of this density error is then compared to the daily RMS of uncertainty in the estimate generated by ODTK. From this difference, a scaling factor is determined to allow for a comparison between different atmospheric models. This scaling factor for one satellite is then used to estimate the density error using the uncertainty of the other satellite, and compared to the original error value. Finally, these scale factors are applied to the uncertainty in atmospheric estimates made for the ANDE satellites to estimate the daily RMS error for these satellites.

3 VERIFICATION OF ESTABLISHED POE DENSITY METRICS

3.1 Definition of Bins

To verify that the code generated is identical to the work completed in Mysore Krishna [12], the cross correlation and RMS difference between the Bruinsma accelerometer derived densities used as a baseline and the density values of interest were calculated. In addition to POE, the accelerometer densities were also compared to the High Accuracy Satellite Drag Model (HASDM) [34], NRLMSISE-00 [11], and Jacchia-71 [6] To ensure that each model worked well for all space weather conditions, the CC and RMS errors were placed into separate bins based on Picone et. al. [11] These bins are given in Table 3.1 below.

Table 3.1: CC and RMS Bin Definitions [11]

Activity Bin	Bin Definition
Low Solar	$F_{10.7} < 75$
Moderate Solar	$75 \leq F_{10.7} < 150$
Elevated Solar	$150 \leq F_{10.7} < 190$
High Solar	$190 \leq F_{10.7}$
Quiet Geomagnetic	$A_p \leq 10$
Moderate Geomagnetic	$10 < A_p \leq 50$
Active Geomagnetic	$50 \leq Ap$

3.2 Results for CHAMP

Table 3.2 shows the CC values previously given for CHAMP, and Table 3.3 shows the CC that was re-calculated using the new code. Table 3.4 then shows the RMS previously given, and Table 3.5 shows the re-calculated RMS.

Table 3.2: Previously Calculated CHAMP CC Values [40]

Bin	Cross Correlation			
	POE derived density	HASDM	NRLMSISE-00	Jacchia-71
Overall	0.934	0.924	0.888	0.886
Low Solar	0.926	0.910	0.880	0.884
Moderate Solar	0.935	0.925	0.881	0.884
Elevated Solar	0.938	0.936	0.907	0.895
High Solar	0.948	0.942	0.903	0.895
Quiet Geomagnetic	0.935	0.923	0.891	0.896
Moderate Geomagnetic	0.932	0.924	0.885	0.874
Active Geomagnetic	0.950	0.941	0.871	0.831

Table 3.3: Recalculated CHAMP CC Values

Bin	Cross Correlation			
	POE derived density	HASDM	NRLMSISE-00	Jacchia-71
Overall	0.935	0.924	0.888	0.891
Low Solar	0.923	0.906	0.876	0.881
Moderate Solar	0.937	0.928	0.883	0.893
Elevated Solar	0.947	0.935	0.906	0.900
High Solar	0.949	0.944	0.901	0.895
Quiet Geomagnetic	0.936	0.925	0.893	0.898
Moderate Geomagnetic	0.934	0.924	0.885	0.882
Active Geomagnetic	0.950	0.940	0.871	0.830

Table 3.4: Previously Calculated CHAMP RMS Values [40]

Bin	Root Mean Square (10^{-12} kg/m^3)			
	POE derived density	HASDM	NRLMSISE-00	Jacchia-71
Overall	0.383	0.400	0.701	0.836
Low Solar	0.322	0.346	0.849	0.925
Moderate Solar	0.354	0.372	0.643	0.663
Elevated Solar	0.526	0.531	0.719	1.027
High Solar	0.573	0.576	0.783	1.434
Quiet Geomagnetic	0.346	0.361	0.745	0.759
Moderate Geomagnetic	0.423	0.441	0.658	0.895
Active Geomagnetic	0.925	0.986	0.551	3.231

Table 3.5: Recalculated CHAMP RMS Values

Bin	Root Mean Square (10^{-12} kg/m^3)			
	POE derived density	HASDM	NRLMSISE-00	Jacchia-71
Overall	0.379	0.398	0.700	0.839
Low Solar	0.324	0.346	0.849	0.908
Moderate Solar	0.357	0.376	0.641	0.675
Elevated Solar	0.471	0.489	0.721	0.975
High Solar	0.574	0.578	0.782	1.457
Quiet Geomagnetic	0.345	0.361	0.745	0.776
Moderate Geomagnetic	0.414	0.435	0.656	0.877
Active Geomagnetic	0.927	0.992	0.550	3.241

3.3 Results for GRACE

Tables 3.6–3.9 show the CC and RMS values before and after re-calculation for GRACE.

Table 3.6: Previously Calculated GRACE CC Values [40]

Bin	Cross Correlation			
	POE derived density	HASDM	NRLMSISE-00	Jacchia-71
Overall	0.885	0.873	0.844	0.839
Low Solar	0.855	0.840	0.822	0.816
Moderate Solar	0.912	0.902	0.863	0.859
Quiet Geomagnetic	0.883	0.869	0.852	0.840
Moderate Geomagnetic	0.891	0.881	0.827	0.836

Table 3.7: Recalculated GRACE CC Values

Bin	Cross Correlation			
	POE derived density	HASDM	NRLMSISE-00	Jacchia-71
Overall	0.889	0.881	0.849	0.852
Low Solar	0.868	0.859	0.832	0.842
Moderate Solar	0.908	0.899	0.861	0.860
Quiet Geomagnetic	0.881	0.873	0.855	0.847
Moderate Geomagnetic	0.908	0.898	0.838	0.864

Table 3.8: Previously Calculated GRACE RMS Values [40]

Bin	Root Mean Square (10^{-12} kg/m^3)			
	POE derived density	HASDM	NRLMSISE-00	Jacchia-71
For all Bins	0.044	0.047	0.089	0.111
Low Solar	0.031	0.031	0.079	0.100
Moderate Solar	0.056	0.060	0.098	0.122
Quiet Geomagnetic	0.036	0.038	0.080	0.096
Moderate Geomagnetic	0.063	0.068	0.109	0.147

Table 3.9: Recalculated GRACE RMS Values

Bin	Root Mean Square (10^{-12} kg/m^3)			
	POE derived density	HASDM	NRLMSISE-00	Jacchia-71
For all Bins	0.048	0.050	0.091	0.117
Low Solar	0.031	0.031	0.079	0.097
Moderate Solar	0.063	0.067	0.101	0.133
Quiet Geomagnetic	0.043	0.045	0.083	0.108
Moderate Geomagnetic	0.057	0.058	0.094	0.123

3.4 Summary

As shown in the above tables, the values for both the cross correlation and root mean square error are generally within 1% of the original values. Any deviations from the values found previously are likely due to a difference in either software version or machine precision. However, as the values are approximately equal to the originals, this is not considered problematic. As a result, the attempt at recreating the data was deemed a success.

4 IMPROVEMENTS TO EXISTING POE DENSITY METRICS

4.1 Merging of Sutton and Bruinsma Accelerometer Data

A few of the patched gaps for CHAMP illustrated in Figure 2.1 are shown below in Figures 4.1–4.3.

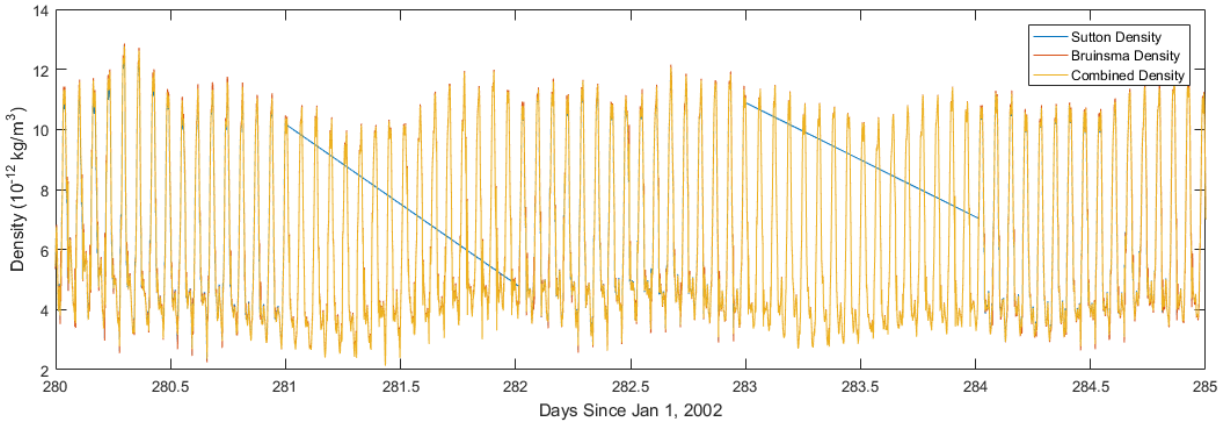

Figure 4.1: Example of Two Patched Gaps in Sutton Density on Oct. 9 and 11, 2002

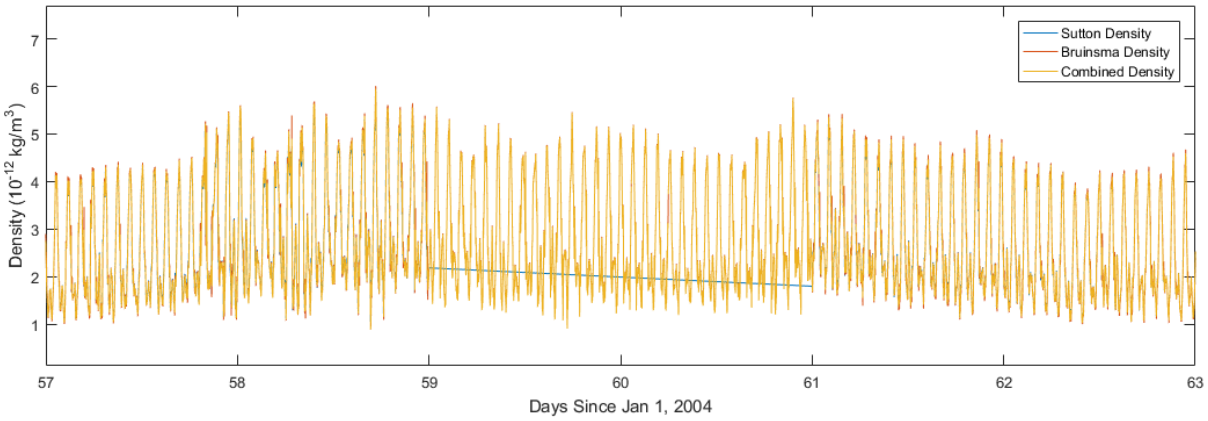

Figure 4.2: Example of Medium-Sized Patched Gap in Sutton Density on Feb 29-Mar 1, 2004

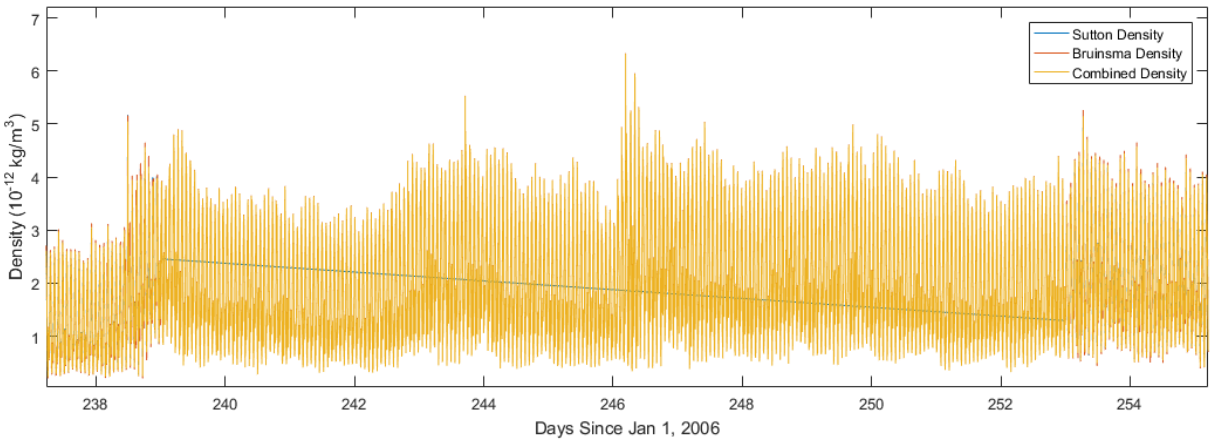

Figure 4.3: Example of Large Patched Gap in Sutton Density from Aug. 28 to Sep. 11, 2006

As can be seen from the above figures, any set of data can be sufficiently patched given a large enough alternative data set.

4.2 CC and RMS from Continuous Data Stream

4.2.1 CHAMP

The following tables show the new values of CC are given for CHAMP in Table 4.1. Next, Table 4.2 shows the RMS values for CHAMP. Finally, Table 4.3 shows the absolute mean percent error for CHAMP, as calculated in Section 2.2.3.

Table 4.1: CHAMP CC Values Using Data from 2001-2010

Bin	Cross Correlation			
	POE derived density	HASDM	NRLMSISE-00	Jacchia-71
Overall	0.970	0.968	0.916	0.901
Low Solar	0.946	0.938	0.892	0.895
Moderate Solar	0.958	0.954	0.895	0.885
Elevated Solar	0.971	0.968	0.916	0.890
High Solar	0.962	0.958	0.885	0.811
Quiet Geomagnetic	0.972	0.970	0.926	0.914
Moderate Geomagnetic	0.966	0.963	0.901	0.884
Active Geomagnetic	0.957	0.950	0.893	0.876

Table 4.2: CHAMP RMS Values Using Data from 2001-2010

Bin	Root Mean Square (10^{-12} kg/m^3)			
	POE derived density	HASDM	NRLMSISE-00	Jacchia-71
Overall	0.454	0.457	0.802	1.050
Low Solar	0.334	0.359	0.838	1.004
Moderate Solar	0.378	0.397	0.602	0.752
Elevated Solar	0.579	0.580	0.930	1.291
High Solar	0.881	0.812	1.419	2.058
Quiet Geomagnetic	0.415	0.417	0.753	0.945
Moderate Geomagnetic	0.488	0.491	0.841	1.131
Active Geomagnetic	0.793	0.801	1.301	1.988

Table 4.3: CHAMP Absolute Mean Percent Error Values Using Data from 2001-2010

Bin	Absolute Mean Percent Error			
	POE derived density	HASDM	NRLMSISE-00	Jacchia-71
Overall	14.1%	14.5%	27.7%	33.7%
Low Solar	18.0%	19.7%	45.7%	52.6%
Moderate Solar	11.7%	12.1%	19.8%	24.4%
Elevated Solar	11.2%	10.5%	18.4%	24.7%
High Solar	19.8%	17.0%	29.7%	41.5%
Quiet Geomagnetic	15.3%	15.8%	30.8%	36.9%
Moderate Geomagnetic	12.2%	12.5%	22.7%	28.4%
Active Geomagnetic	13.2%	13.0%	23.7%	32.7%

4.2.2 **GRACE**

Tables 4.4-4.6 illustrate the same cross correlation, RMS and absolute mean percent error values for GRACE.

Table 4.4: GRACE CC Values Using Data from 2002-2010

Bin	Cross Correlation			
	POE derived density	HASDM	NRLMSISE-00	Jacchia-71
Overall	0.931	0.925	0.871	0.855
Low Solar	0.918	0.911	0.860	0.848
Moderate Solar	0.924	0.917	0.863	0.848
Quiet Geomagnetic	0.959	0.954	0.910	0.889
Moderate Geomagnetic	0.889	0.882	0.822	0.795
Active Geomagnetic	0.954	0.943	0.870	0.872

Table 4.5: GRACE RMS Values Using Data from 2002-2010

Bin	Root Mean Square (10^{-12} kg/m^3)			
	POE derived density	HASDM	NRLMSISE-00	Jacchia-71
Overall	0.068	0.072	0.102	0.137
Low Solar	0.034	0.035	0.076	0.102
Moderate Solar	0.080	0.085	0.113	0.151
Quiet Geomagnetic	0.041	0.044	0.077	0.100
Moderate Geomagnetic	0.102	0.107	0.134	0.180
Active Geomagnetic	0.148	0.170	0.238	0.341

Table 4.6: GRACE Absolute Mean Percent Error Values Using Data from 2002-2010

Bin	Absolute Mean Percent Error			
	POE derived density	HASDM	NRLMSISE-00	Jacchia-71
Overall	22.1%	23.4%	45.2%	50.2%
Low Solar	25.8%	27.6%	57.9%	65.4%
Moderate Solar	20.3%	21.3%	38.8%	42.6%
Quiet Geomagnetic	19.3%	20.7%	40.5%	44.5%
Moderate Geomagnetic	28.7%	29.7%	55.8%	63.1%
Active Geomagnetic	20.5%	21.6%	44.8%	51.8%

4.3 Summary

Overall, after recalculating the RMS and CC for the CHAMP and GRACE missions, a noticeable improvement has been made in the cross correlation of the data sets with the accelerometer data. Overall, incorporating a larger data set provides a much clearer picture of the performance of these metrics, providing a better assessment of which method most accurately captures the atmospheric densities encountered by the satellites. The RMS values, in general, increased from the baseline values calculated by Mysore Krishna [12]. The inclusion of the Sutton data has allowed for a more comprehensive comparison overall. The omitted values from the previous analysis have inadvertently undervalued the errors inherent in the model.

The baseline atmospheric models, Jacchia and NRLMISE, generally provide a worse result for the CHAMP and GRACE satellites. Both the CC and RMS values returned for these atmospheric models perform much worse than the HASDM and the POE densities. In ranking the atmospheric density models, Jacchia-71 is the lowest performer, followed by NRLMSISE-00, then HASDM, and finally the POE derived densities. In general, the POE derived atmospheric densities are still most closely match the accelerometer data in most cases for both satellites.

5 DRAG COEFFICIENTS AND EFFECTIVE AREAS

This chapter discusses the drag coefficients as calculated in Section 2.3. For the ANDE missions, these drag coefficients are then plotted with respect to time. Next, a smoothing process is done to the data to allow better comparison between each of the separate drag coefficient values. The data is smoothed using a standard moving average low pass filter with a span of 1 day (1441 minutes). The span length is not exactly 1 day, as the smoothing process requires an odd number of measurements centered on the current value. Finally, in each section, the drag coefficients are compared to one another by selecting a baseline drag coefficient model that fell predominantly in the center of the rest of the data. The model selected as the baseline was the Temkin CLL model.

For the CHAMP and GRACE satellite missions, the atmospheric densities and the satellite area must be known as inputs to the OD process. As a result, both the drag coefficient and the area normal to the flow must be known.

5.1 ANDE Missions

Figure 5.1 below illustrates the raw drag coefficient data collected for the ANDE-RR MAA satellite mission. Next, Figure 5.2 shows the smoothed drag coefficients, which are smoothed as discussed in the previous section. Finally, Figure 5.3 shows the comparison of the respective atmospheric densities. Figures 5.4-5.6 show the same information for the ANDE-RR Fcal satellite, and then Figures 5.7-5.9 and Figures 5.10-5.12 provide the same information for the ANDE-2 Satellites Castor and Pollux respectively. Using these atmospheric densities, the effective area of the satellites can be calculated using Equation 2.19.

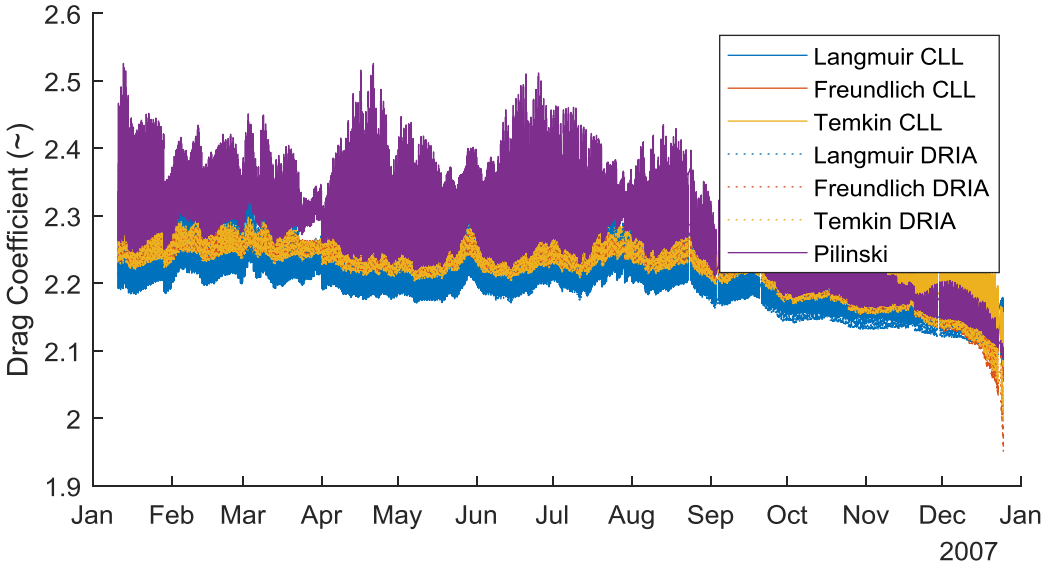

Figure 5.1: ANDE-RR MAA Drag Coefficients

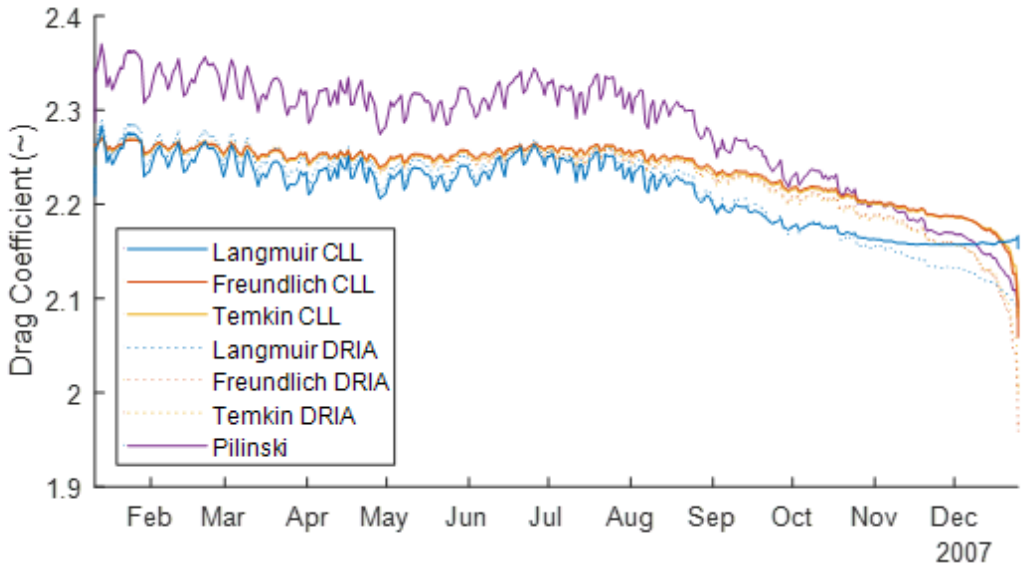

Figure 5.2: ANDE-RR MAA Smoothed Drag Coefficients

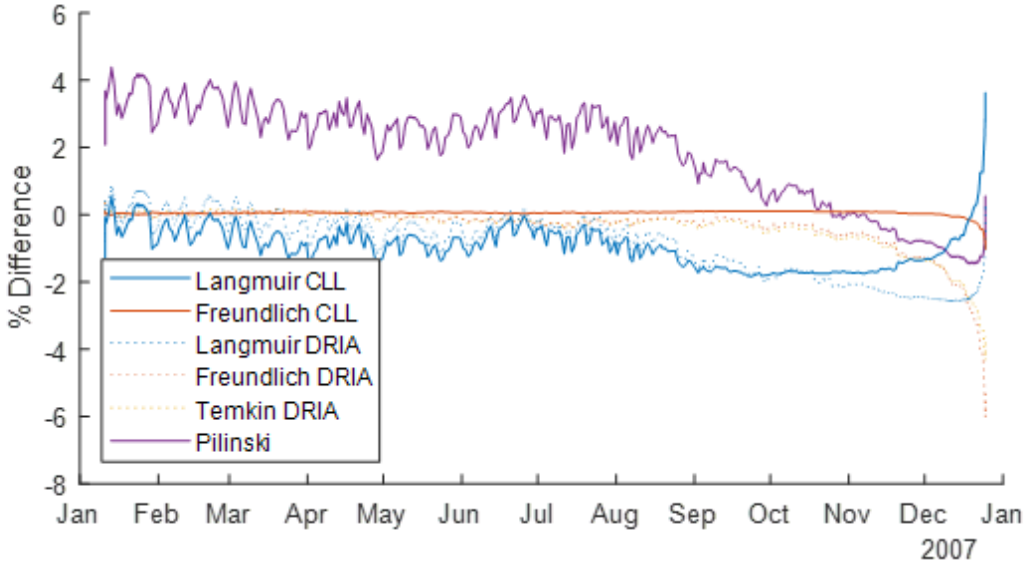

Figure 5.3: ANDE-RR MAA Smoothed Drag Coefficients Percent Difference Using Temkin CLL as Baseline

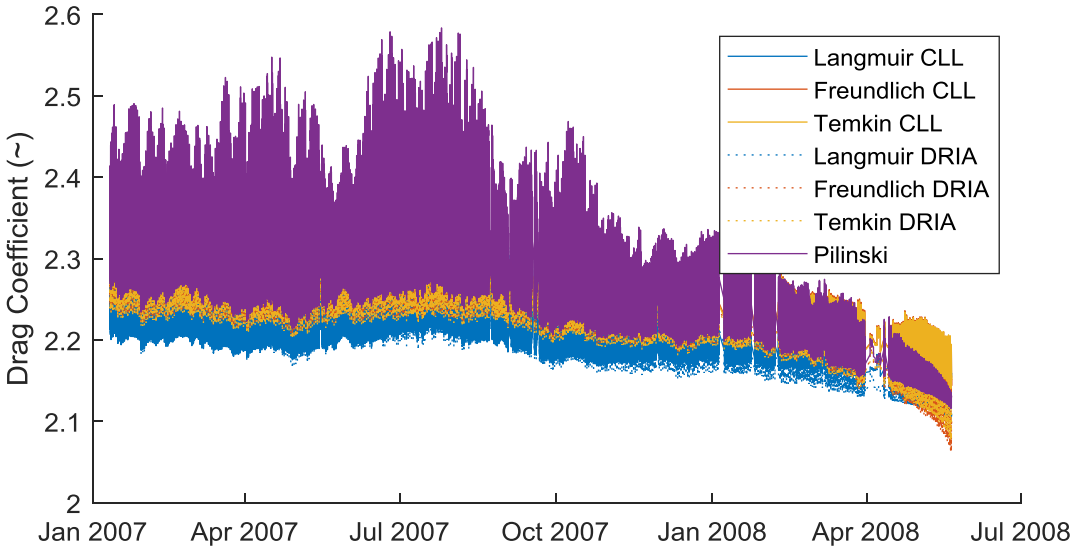

Figure 5.4: ANDE-RR Fcal Drag Coefficients

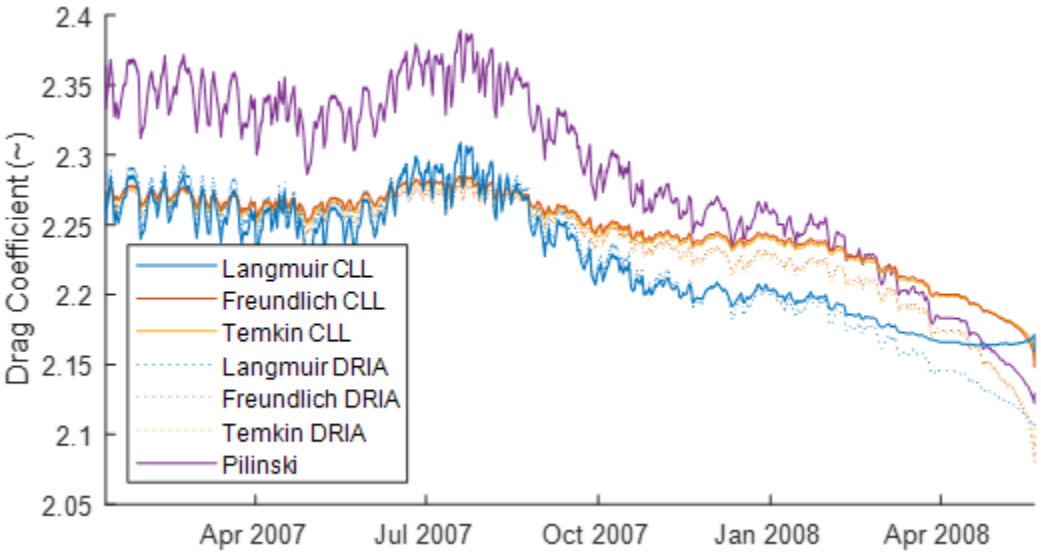

Figure 5.5: ANDE-RR Fcal Smoothed Drag Coefficients

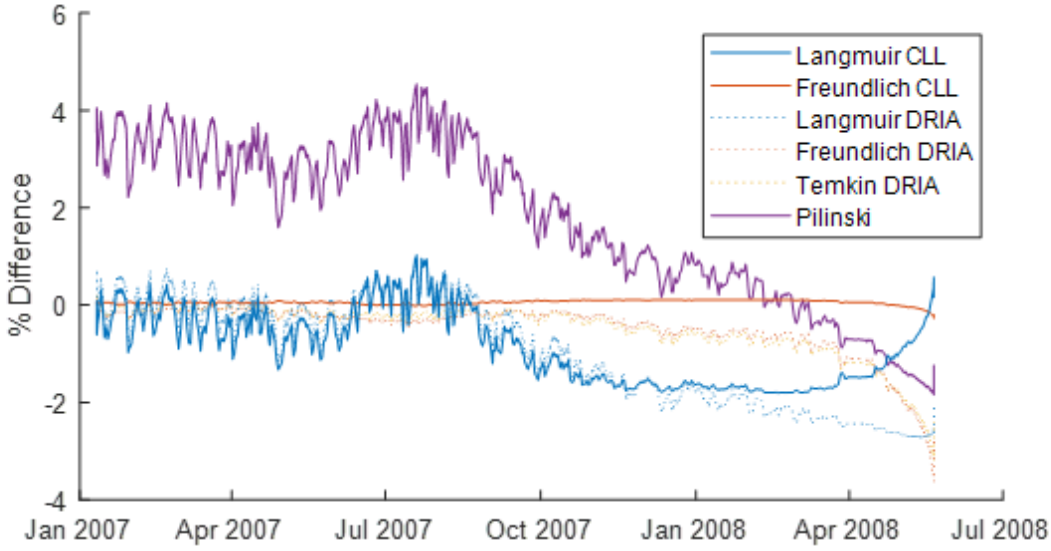

Figure 5.6: ANDE-RR Fcal Smoothed Drag Coefficients Percent Difference Using Temkin CLL as Baseline

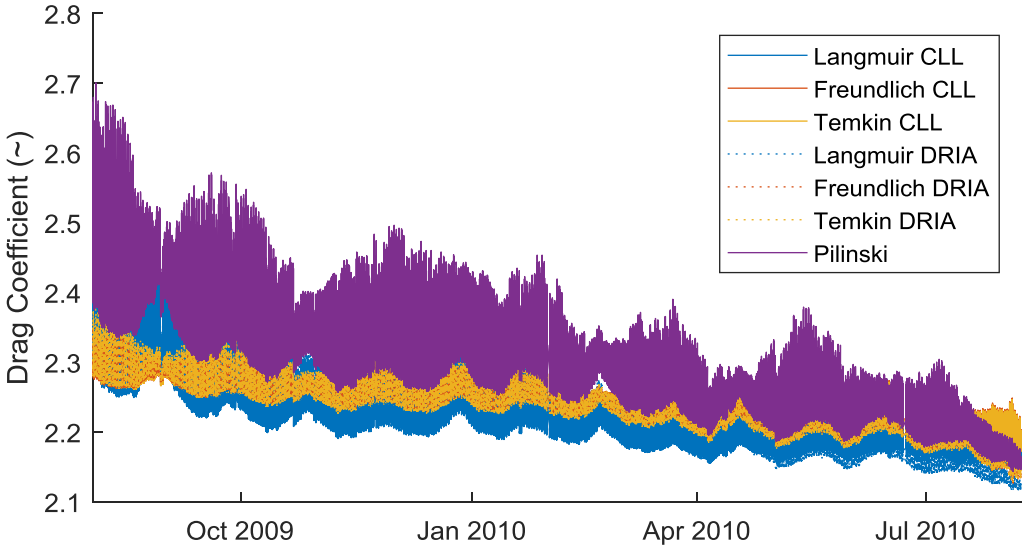

Figure 5.7: ANDE-2 Castor Drag Coefficients

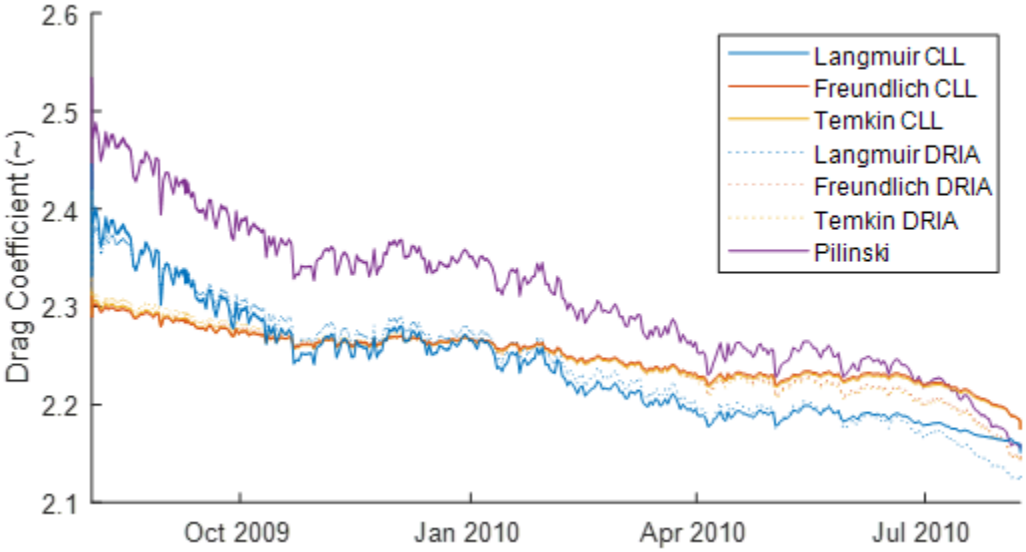

Figure 5.8: ANDE-2 Castor Smoothed Drag Coefficients

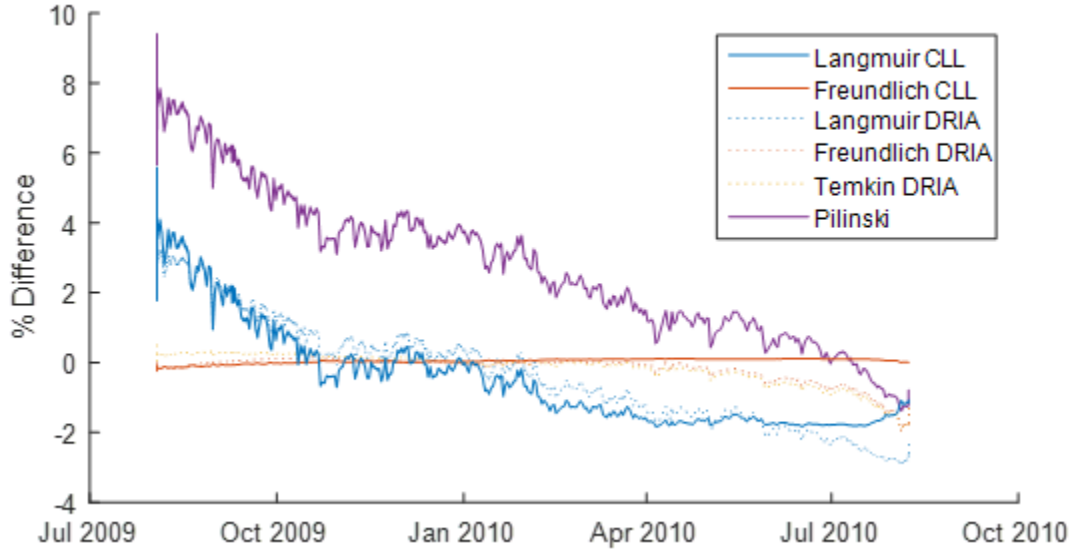

Figure 5.9: ANDE-2 Castor Smoothed Drag Coefficients Percent Difference Using Temkin CLL as Baseline

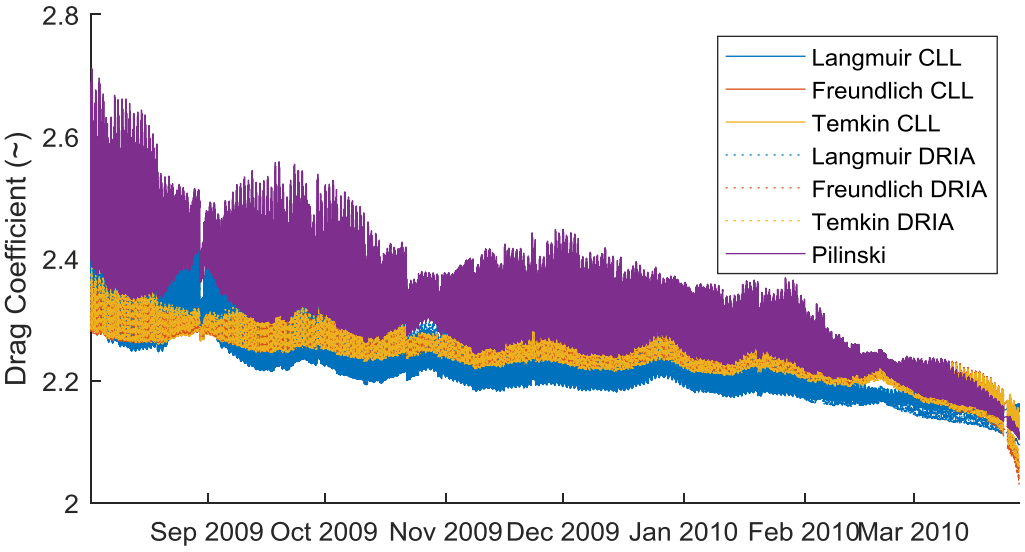

Figure 5.10: ANDE-2 Pollux Drag Coefficients

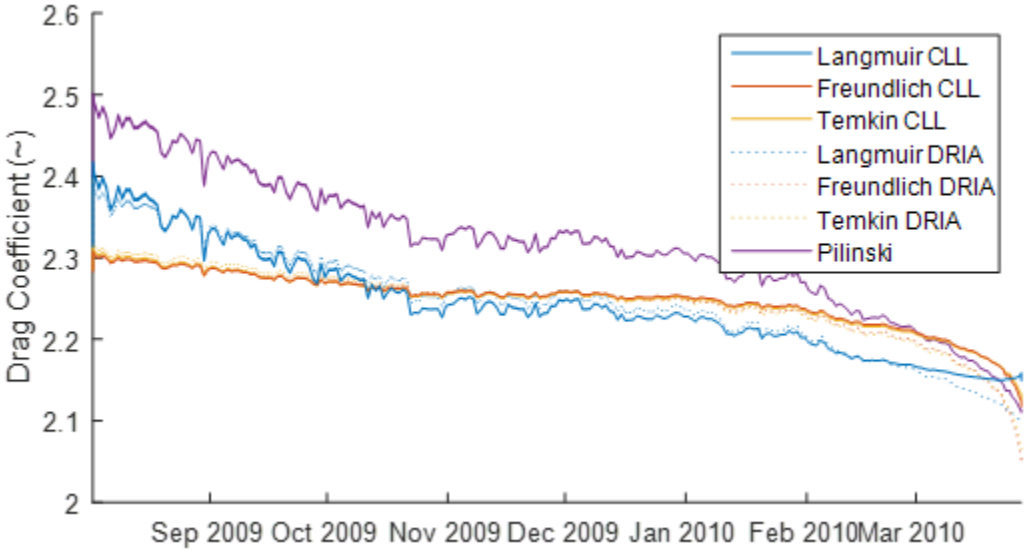

Figure 5.11: ANDE-2 Pollux Smoothed Drag Coefficients

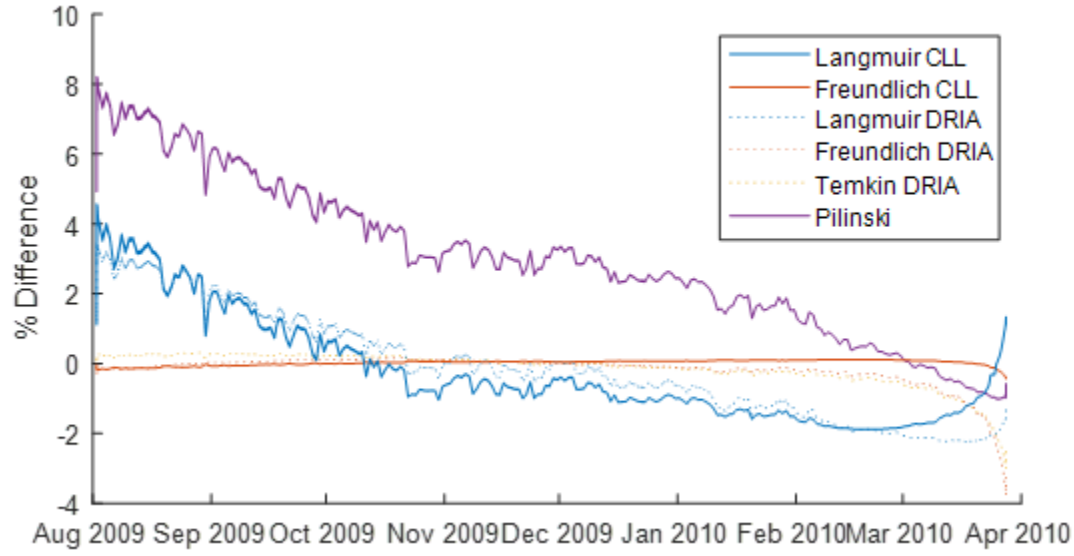

Figure 5.12: ANDE-2 Pollux Smoothed Drag Coefficients Percent Difference Using Temkin CLL as Baseline

As can be seen from the above figures, the Pilinski and Langmuir drag coefficient models tend to follow the same trend line with a slight offset. This is due to these two models using a

similar adsorption model. In the beginning of each satellite's life, the Pilinski and Langmuir drag coefficients provide a higher estimate of the drag coefficients as compared to the Temking and Freundlich models. The Temkin and Freundlich adsorption models tend to follow a very similar trend throughout, showing a near zero percent difference when compared to Temkin CLL. At the end of the satellite's life, the percentage of coverage trends toward an effective accommodation coefficient of 1. As a result, they all tend to converge to a similar value near the end of the life.

Another aspect to note is that the ANDE-RR satellites show less variation between the various methods. This is likely due to the constants that were used in the generation of the drag coefficients were better suited to the ANDE-RR mission than the ANDE-2 mission. Essentially, the space weather conditions used to estimate the empirical constants in the drag coefficient models were more similar to the lifetime of the ANDE-RR satellites than the ANDE-2 satellites' lifetime.

To validate the drag coefficients as discussed in this section, the tables found in Moe et. al. [18] provides approximate values for the satellite drag coefficients. However, as discussed in Section 1.5, the lower bound of the accommodation coefficient is 0.90. This is in direct conflict with the early measurements for each satellite, which have an accommodation coefficient of around 0.83 in the beginning of the mission for the ANDE-2 satellites. Thus, extrapolation to these values is necessary. Table 5.1 below illustrates the approximate values found for each satellite near the beginning and end of their lives, given their accommodation coefficient and the ambient temperature.

Table 5.1: Drag Coefficients Derived from Literature

	ANDE-RR		ANDE-2	
	MAA	Fcal	Castor	Pollux
Beginning of Life	2.33	2.33	2.34	2.34
End of Life	2.09	2.12	2.19	2.09

As can be seen in the above table, the drag coefficients for each of the satellites generally fall within these bounds. However, for several of the Pilinski drag coefficients found in the early portions of the ANDE-2 satellite missions are seen to be above this value. This is likely due to the Pilinski derived drag coefficients not being valid for accommodation coefficient values less than 0.85. This is further reflected in the differences between drag coefficient models in Figures 5.9 and 5.12. Early in the satellite's lifetime, the difference between the Pilinski values and the other drag coefficient models are much higher than later in the satellite missions.

To ensure that the free molecular flow assumption holds for the entire lifetime of the satellite, the Knudson number is calculated at the end of life for each satellite. Table 5.2 below shows the final Knudsen numbers for each of the ANDE satellites.

Table 5.2: Final Knudsen Number for Each ANDE Satellite

ANDE-2 Castor	ANDE-2 Pollux	ANDE-RR MAA	ANDE-RR Fcal
2933	505	117	3989

As seen in the above table, the Knudson number remains above 10 even at the end of each satellites data set. As a result, the free molecular flow assumption holds, even at the last tracked point for each satellite. If the satellites were tracked even lower into the atmosphere, however, this assumption would no longer hold, and the results would be much more suspect.

5.2 CHAMP and GRACE

Figure 5.13 illustrates the drag coefficients provided in Mehta et. al. for the CHAMP satellite. Next, Figure 5.14 shows the area normal to the flow. Figures 5.15 and 5.16 then illustrate the drag coefficient and normal area respectively for the GRACE-A satellite.

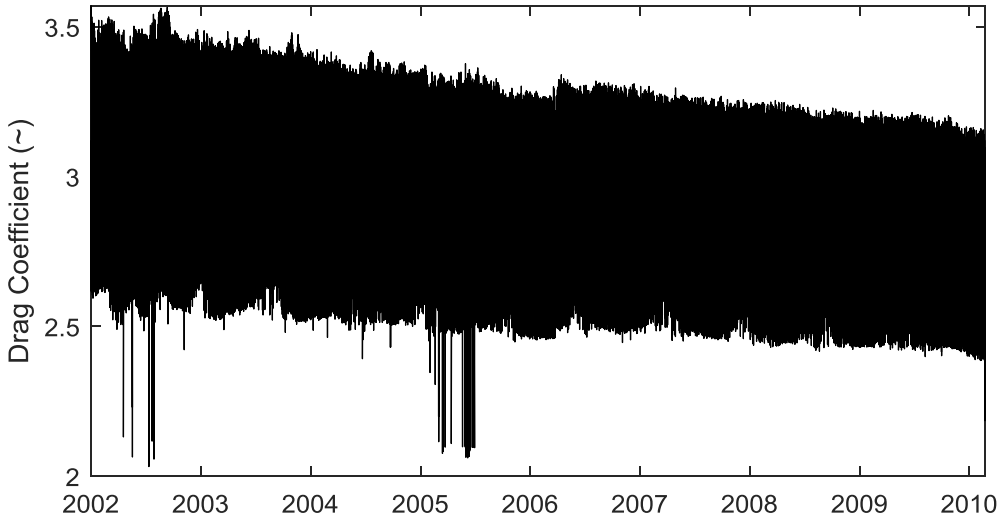

Figure 5.13: CHAMP Drag Coefficients

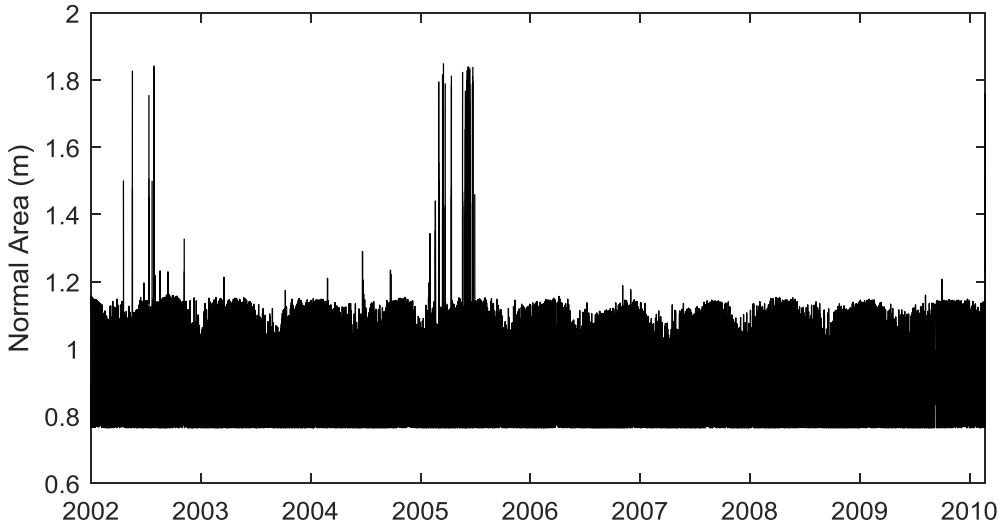

Figure 5.14: CHAMP Normal Areas

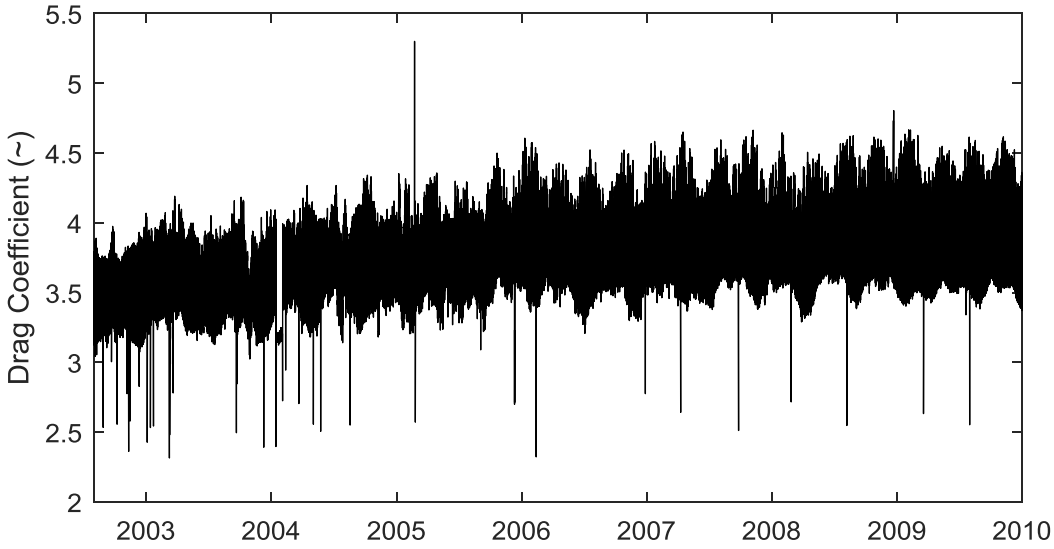

Figure 5.15: GRACE Drag Coefficients

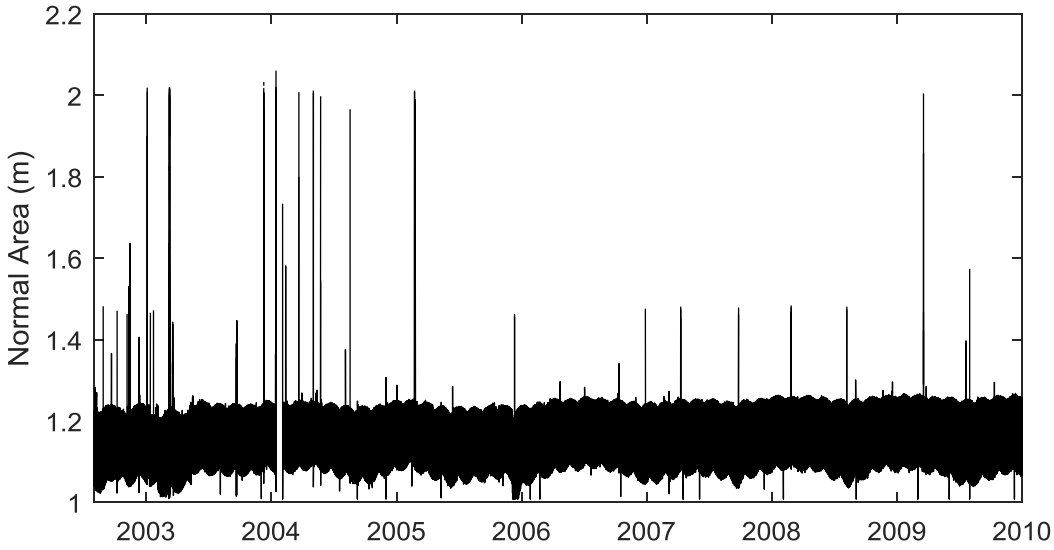

Figure 5.16: GRACE Normal Areas

The normal areas for the CHAMP and GRACE satellites are consistent with the known geometry of the respective satellites. The spikes in the data for both the CHAMP and GRACE satellites are likely due to errors in the raw data used to generate the drag coefficients and normal areas. As a check on these values, the highest and lowest possible normal areas will provide the upper and lower limits on Figures 5.14 and 5.16. Figures 1.4 and 1.6 in Section 1.6 demonstrate

the basic geometry of the CHAMP and GRACE satellites respectively. In general, the CHAMP and GRACE satellites orbited with their trapezoidal face pointed into the flow with minor deviations. This configuration corresponds to the smallest area presented to the flow. Conversely, the largest possible area presented would be with the top or bottom of the satellites pointed toward the flow. Table 5.3 below shows the ranges of areas for the CHAMP and GRACE satellites.

Table 5.3: Upper and Lower Bounds for CHAMP and GRACE Area

	Smallest Area	Largest Area
CHAMP	0.75 m	6.88 m
GRACE	0.95 m	6.05 m

As expected, the lower bound for the CHAMP satellite sits at exactly 0.75 meters. The GRACE satellite generally was slightly above this smallest area, but this is likely due to the requirement that the satellite point a radio frequency range finder to its sister satellite for the duration of the mission. The orientation requirement was not driven in this case by reducing drag, but by pointing an instrument.

The drag coefficients for the CHAMP and GRACE satellites, although higher than the ANDE satellites, are not outside the realm of possibility. As seen with the ANDE satellites, the accommodation coefficient is an inverse function of the satellite's altitude. This inverse relationship does affect the estimated drag coefficient. However, the primary source of the higher drag coefficient is due to the geometry of the spacecraft. The CHAMP and GRACE satellites are trapezoidal prisms instead of spheres, as their primary mission focus was not to estimate atmospheric drag. As seen in Moe et. al. [18], the closest geometry to these satellites, the cylinder with its circular face in the flow, has a much higher drag coefficient than the spherical shape. Finally, the spikes in the drag coefficients for both satellites correspond to the spikes in the

normal areas. In these cases, the drag coefficient is correlated to the projected area of the satellite, so a large spike in one data set corresponds to a large spike in the other.

6 ATMOSPHERIC DENSITY RESULTS USING EFFECTIVE AREAS

This section provides the results of using the effective areas from the previous section, along with the SLR and RSO data collected for the ANDE, and CHAMP and GRACE satellites respectively, to calculate the atmospheric densities using the method outlined in Sections 2.4 and 2.5. In the case of the CHAMP and GRACE satellites, the atmospheric densities are not calculated for the entire life of the satellites, but instead examined for the years 2007 and 2009 to provide a comparison to the ANDE-RR and ANDE-2 satellite missions respectively.

6.1 ANDE Missions

Figure 6.1 below illustrates the raw atmospheric density for the ANDE-RR MAA satellite. Using the same smoothing process as discussed in Section 5.1, this atmospheric density is then smoothed using a 1-day interval, which is shown in Figure 6.2. Finally, Figure 6.3 shows the atmospheric densities compared to the Temkin CLL baseline density established in the previous section. Figures 6.4-6.6 and Figures 6.7-6.9 then illustrate the same sets of atmospheric densities for the ANDE-2 satellites Castor and Pollux, respectively. The ANDE-RR Fcal satellite has been omitted due to the suspect nature of the raw SLR data collected. In this case, the satellite's estimated velocity was too low when added to ODTK and was predicted to reenter in a single orbit.

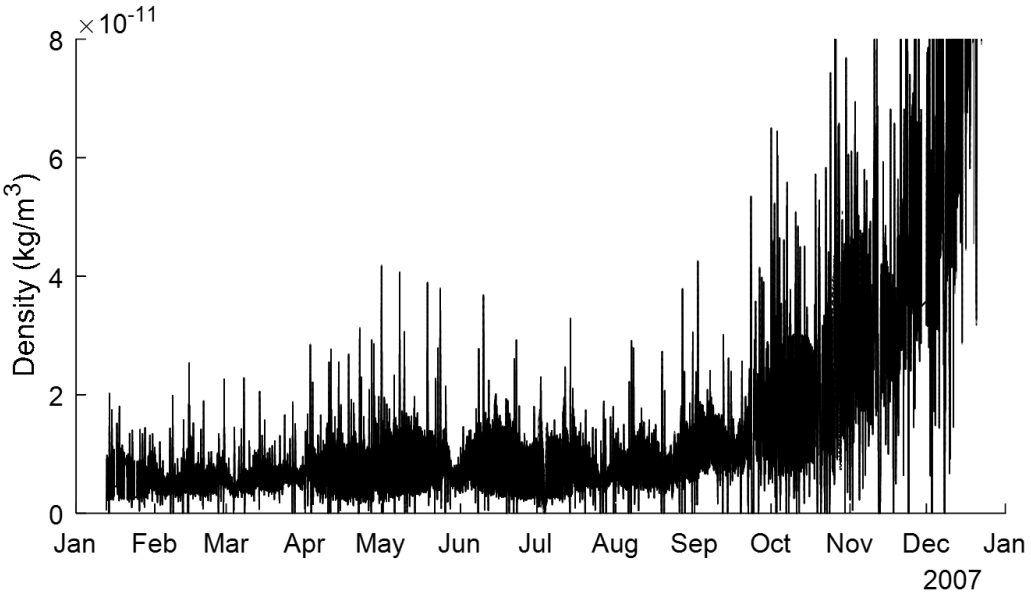

Figure 6.1: ANDE-RR MAA Atmospheric Density Estimates

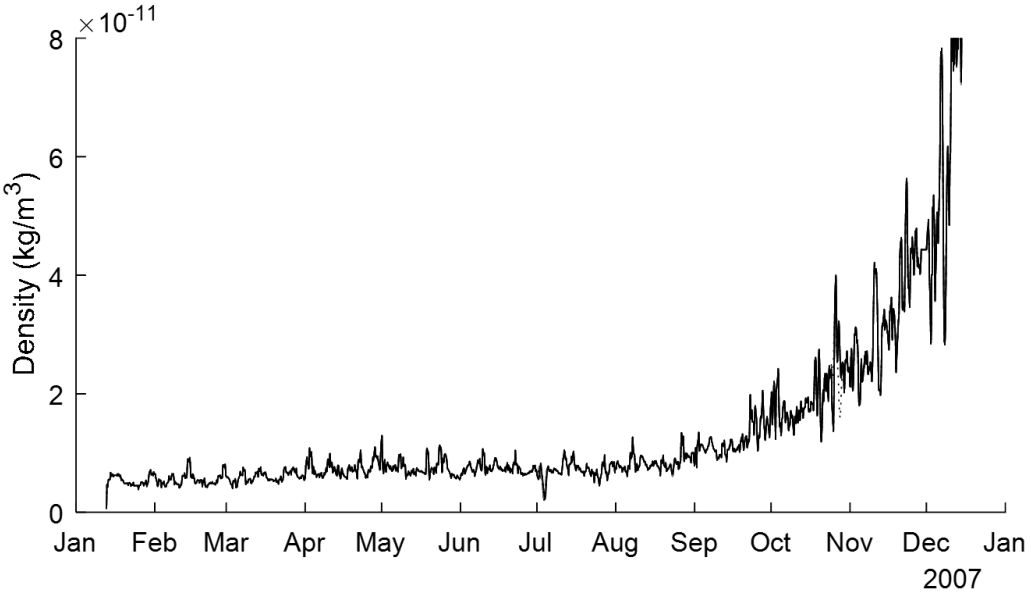

Figure 6.2: ANDE-RR MAA Smoothed Atmospheric Density Estimates

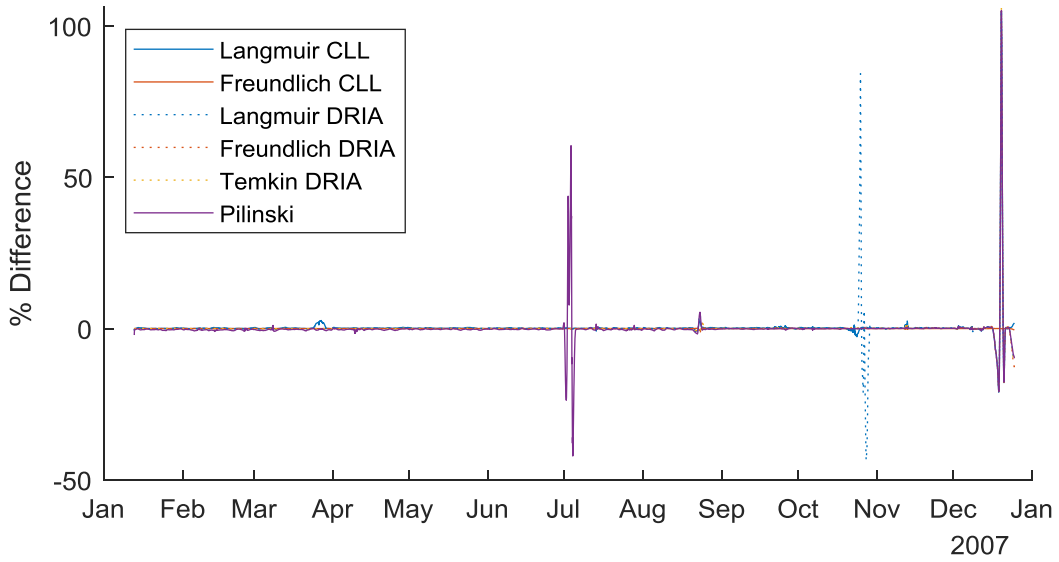

Figure 6.3: ANDE-RR MAA Percent Difference Between Atmospheric Density Estimates by CD Method using Temkin CLL as Baseline

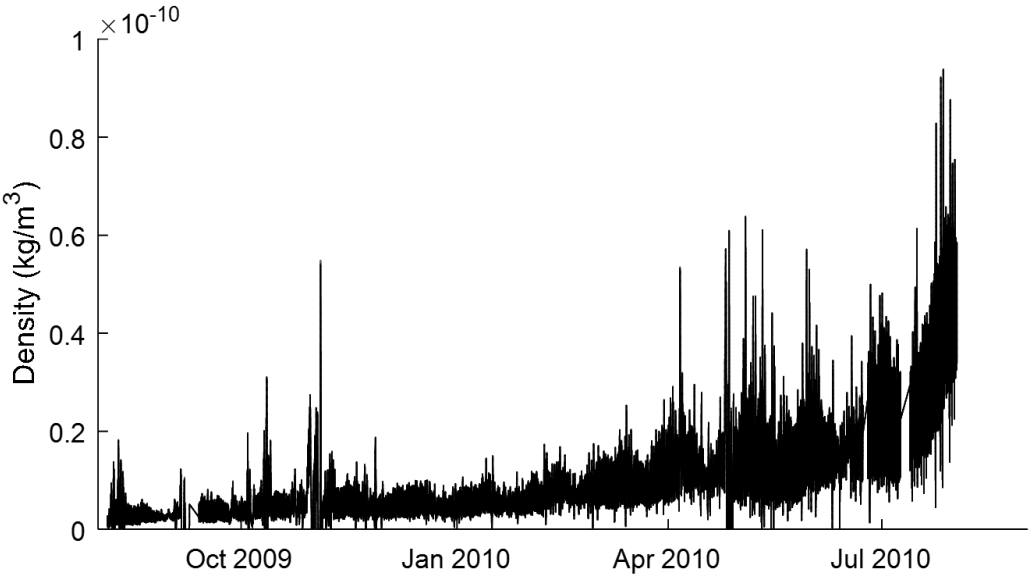

Figure 6.4: ANDE-2 Castor Atmospheric Density Estimates

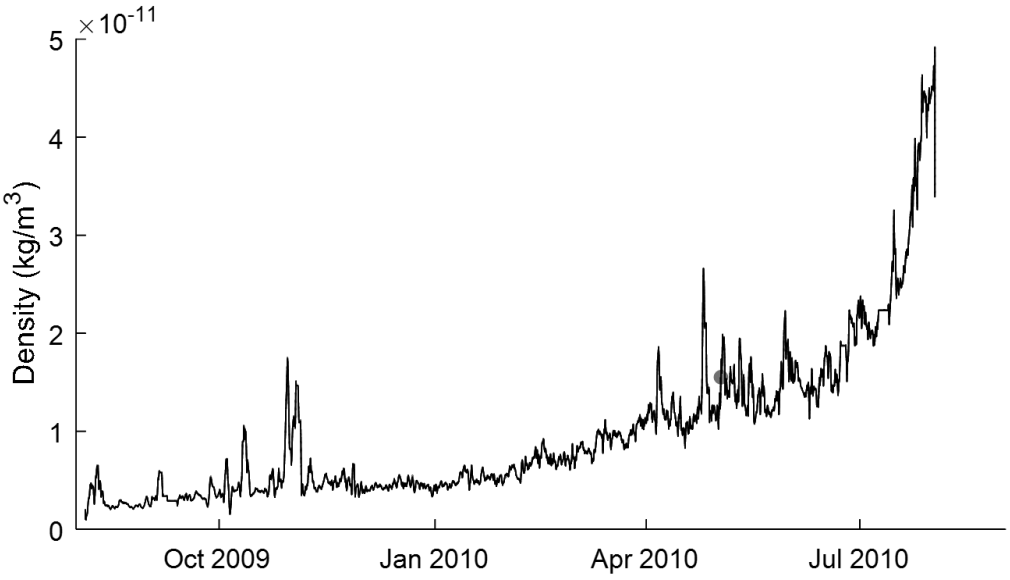

Figure 6.5: ANDE-2 Castor Smoothed Atmospheric Density Estimates

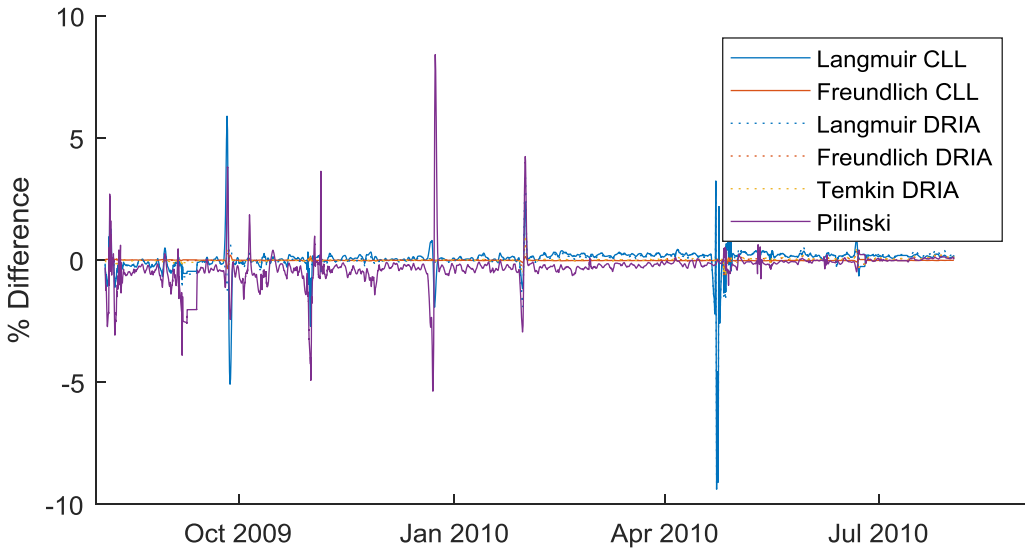

Figure 6.6: ANDE-2 Castor Percent Difference Between Atmospheric Density Estimates by CD Method using Temkin CLL as Baseline

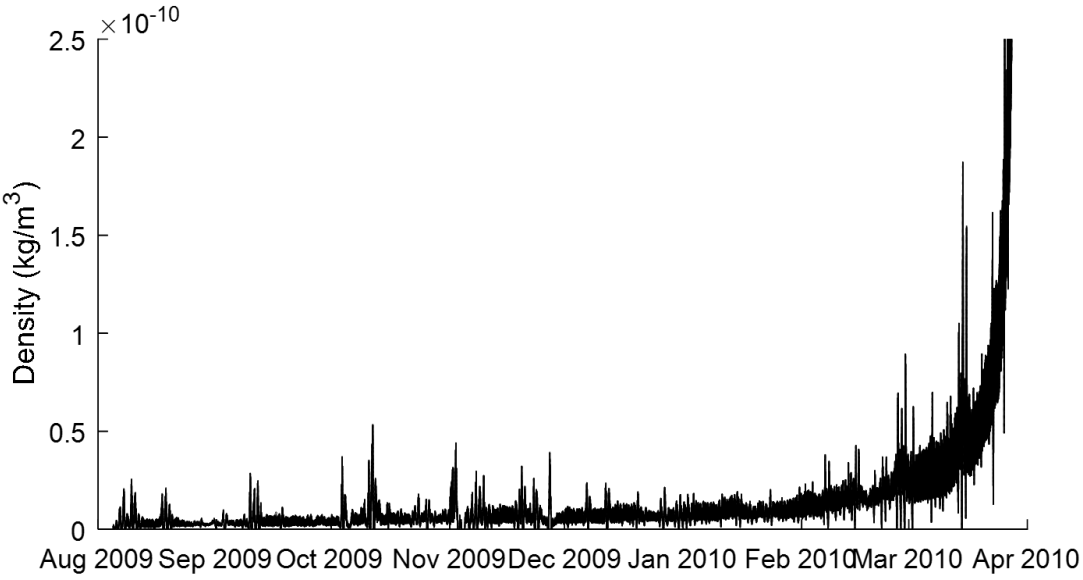

Figure 6.7: ANDE-2 Pollux Atmospheric Density Estimates

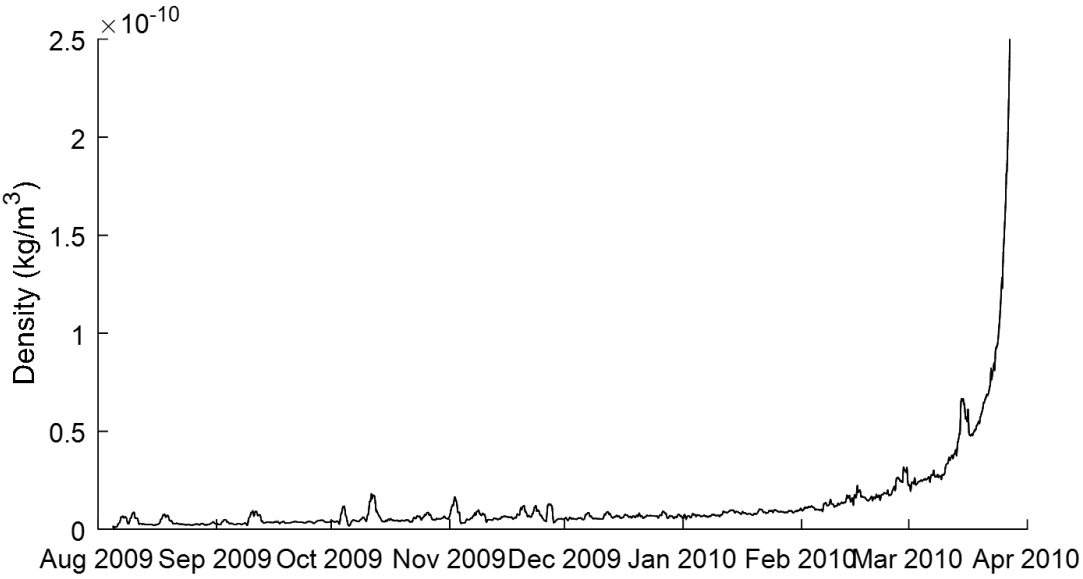

Figure 6.8: ANDE-2 Pollux Smoothed Atmospheric Density Estimates

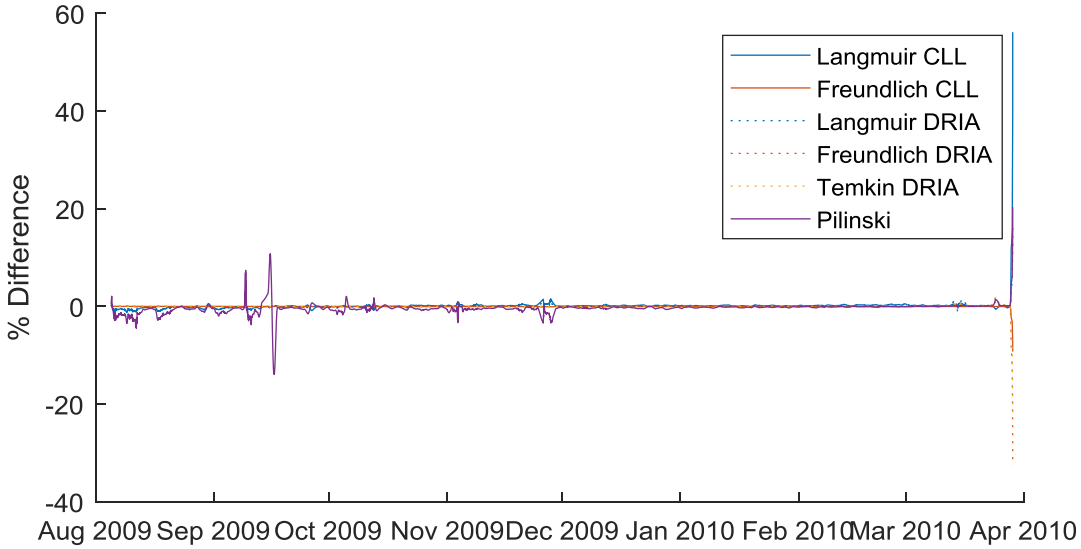

Figure 6.9: ANDE-2 Pollux Percent Difference Between Atmospheric Density Estimates by CD Method using Temkin CLL as Baseline

Across the board, each of the ANDE satellites show a similar trend. At the beginning of their lives, they all experience approximately the same atmospheric densities. This is expected due to the initial conditions being similar between the ANDE-RR and ANDE-2 missions, as the ANDE-RR mission is a risk reduction mission used to test the ANDE-2 hardware and deployment conditions. Therefore, in each case, the conditions they experience should be similar, which is shown by the data.

Examining the difference between each of the drag coefficient methods, it can be seen that for most of the life of the satellites, the effect of each of these different drag coefficient models is imperceptible without a large amount of magnification. This leads to the percent comparisons found in Figures 6.3, 6.6, and 6.9. The atmospheric densities found for each of the satellites in general for each of the drag coefficient models fall within about 1% of each other, save for a few

spikes in the models that use the Langmuir isotherm. In these cases, the spikes are approximately bound within a 10% envelope for the ANDE-2 missions.

The cases where these spikes are not bounded by the 10% envelope are at the end of life for the ANDE-2 Pollux mission. In this case, the satellite is reentering the atmosphere, which causes minute differences in drag coefficient to be amplified dramatically. This can also be seen at the end of life for the ANDE-RR MAA satellite. The ANDE-2 Castor satellite does not show this spike at the end of its life due to the end of this satellites life not captured on this chart. The raw data used to calculate the atmospheric density cuts out before re-entry for this satellite.

Finally, to estimate the sensitivity of the atmospheric density estimates to the changes in drag coefficient, the atmospheric density was estimated again for September 21, 2009 for the ANDE satellite using only the average drag coefficient for the day. The comparison was made for this day, as it provided a time frame with a large amount of SLR data to be processed. This value was then compared to the estimate found using the full set of drag coefficients. Figure 6.10 below illustrates the percent difference between these two values over the course of a day.

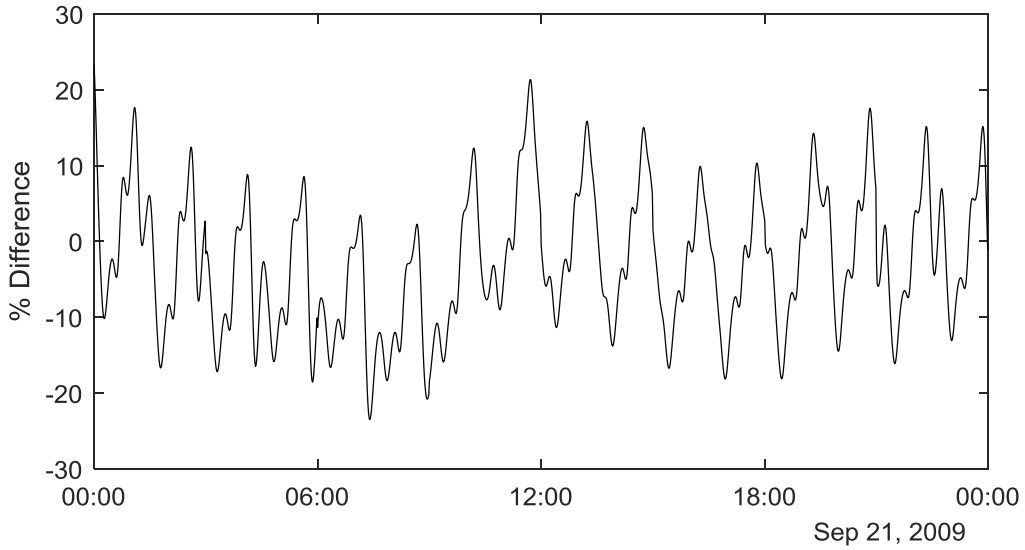

Figure 6.10: Percent Change in Estimated Atmospheric Density for ANDE-2 Castor Using a One-Day Average of Drag Coefficient Compared to Previous Results.

As can be seen in the above figure, the changes in drag coefficient over the course of a day have a strong effect on the estimated atmospheric density. This trend line exists across the board for all drag coefficient models studied. In all cases, the percent change between the daily average of drag coefficient and the full-rate data was as much as 20 percent in either direction. This shows that averaging the drag coefficient is not providing a suitable estimate of the atmospheric density, and a finer C_D model will net a much different result.

6.2 CHAMP and GRACE

Figure 6.11 shows the estimated atmospheric density for the CHAMP satellite for 2007. These results are then smoothed using 1-day averages and plotted in Figure 6.12 to show a clearer picture of the long-term variations. Figures 6.13 and 6.14 then show the results for CHAMP for 2009. Next, Tables 6.1-6.4 show the cross correlation and RMS respectively for the density estimates using the newly calculated drag coefficients and normal areas for 2007 and 2009 compared to the previously estimated values for the respective years, as shown in Section 4.2.1.

These tables also show the percent change between the new and previously calculated estimates. Figures 6.15-6.18 then show the same results for the GRACE satellite for 2009, and Tables 6.5-6.8 provide the same comparison as was completed for CHAMP.

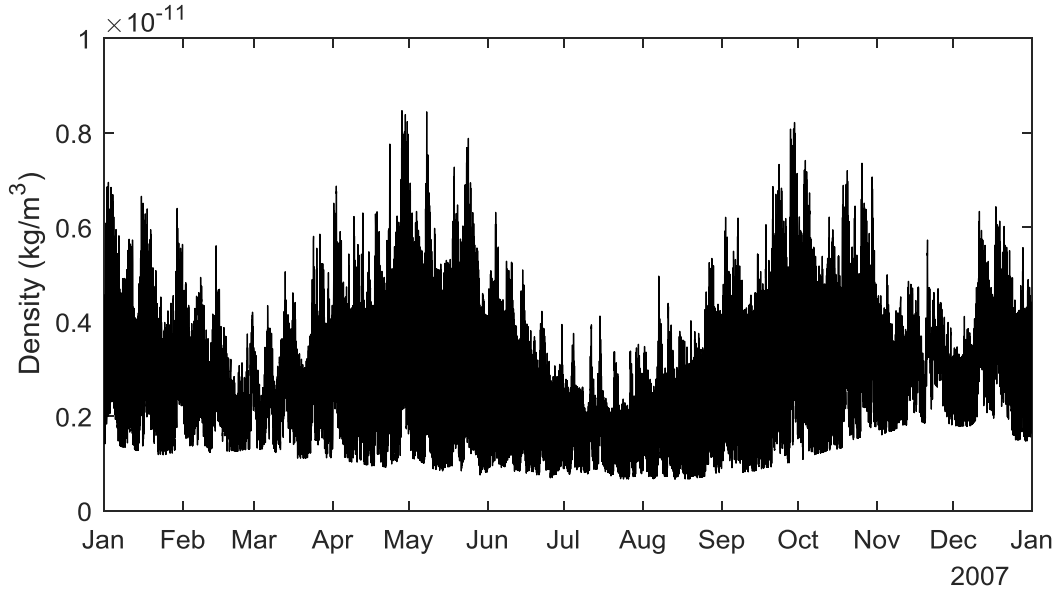

Figure 6.11: CHAMP Atmospheric Density Estimates, 2007

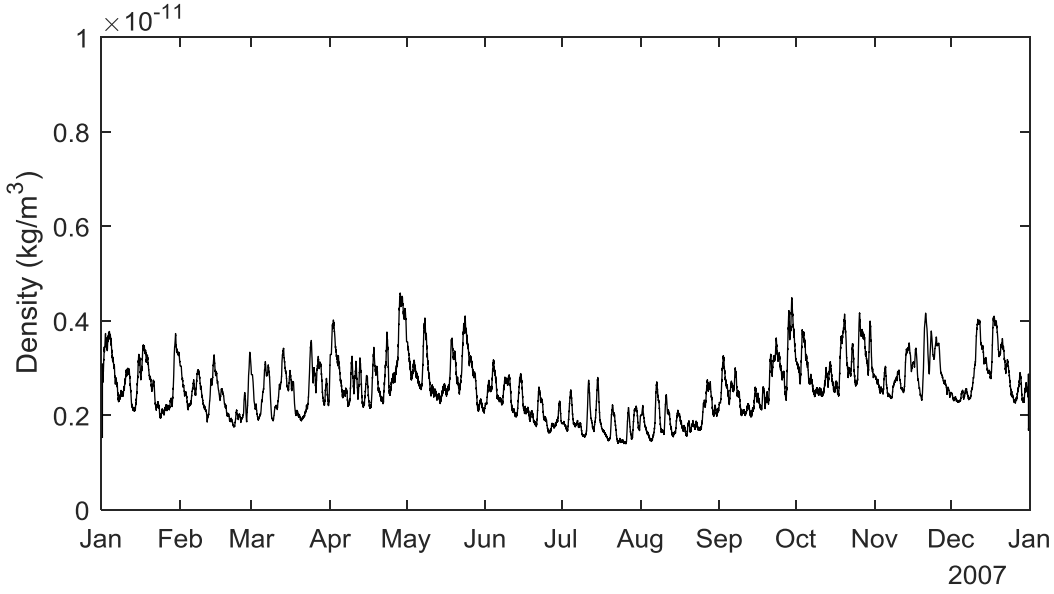

Figure 6.12: CHAMP Smoothed Atmospheric Density Estimates, 2007

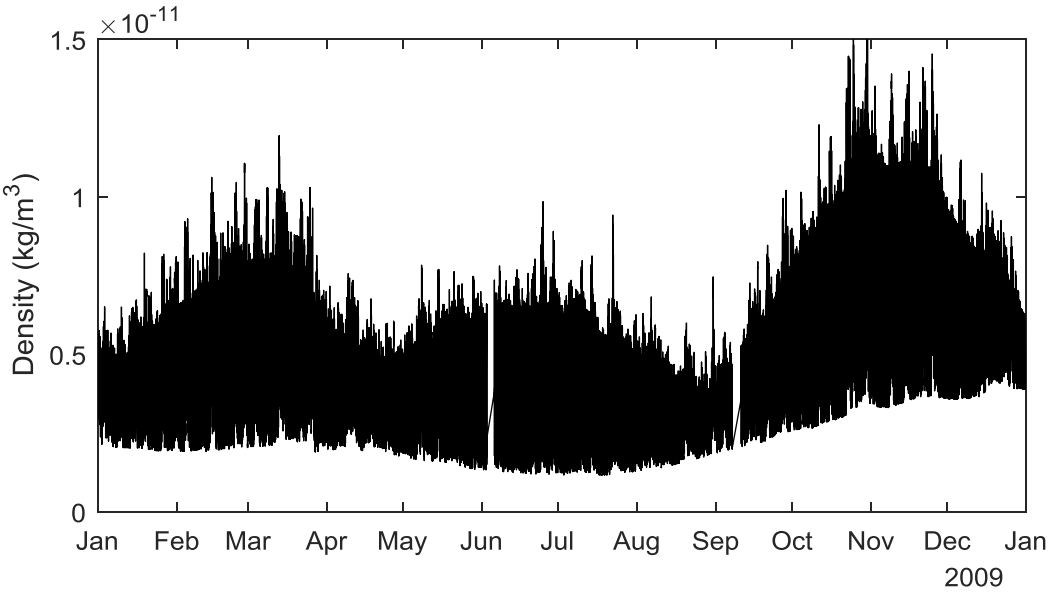

Figure 6.13: CHAMP Atmospheric Density Estimates, 2009

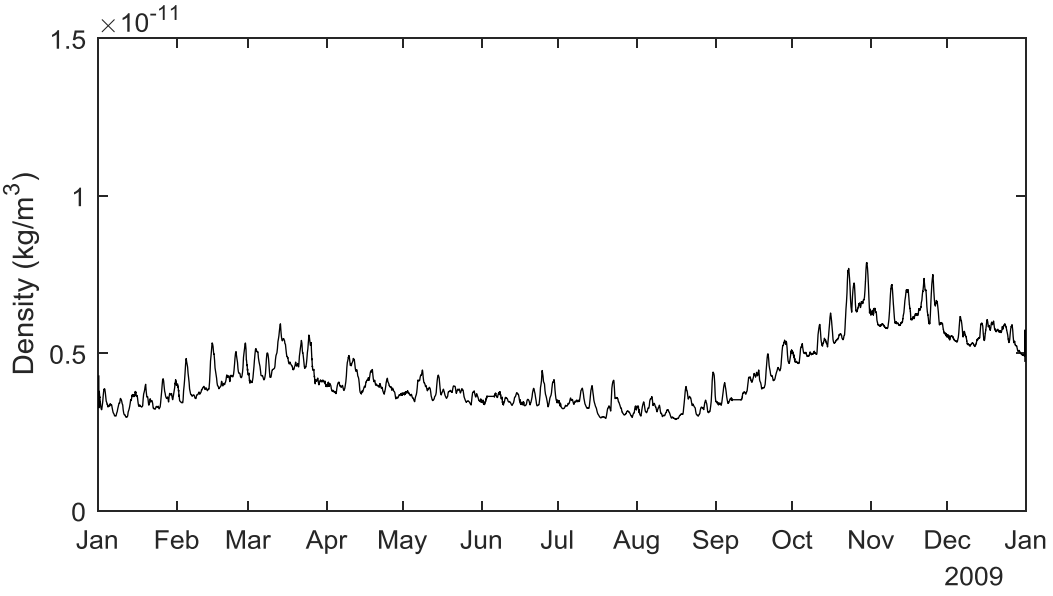

Figure 6.14: CHAMP Smoothed Atmospheric Density Estimates, 2009

Table 6.1: Cross Correlation Comparison, CHAMP 2007

Bin	Cross Correlation		
	POE Given CD	POE Estimated CD	% Change
Overall	0.943	0.944	-0.106%
Low Solar	0.942	0.942	0.000%
Moderate Solar	0.946	0.947	-0.106%
Quiet Geomagnetic	0.943	0.945	-0.317%
Moderate Geomagnetic	0.939	0.940	-0.106%

Table 6.2: RMS Comparison, CHAMP 2007

Bin	Root Mean Square (10^{-12} kg/m^3)		
	POE Given CD	POE Estimated CD	% Change
Overall	0.258	0.303	-14.9%
Low Solar	0.256	0.301	-15.0%
Moderate Solar	0.265	0.307	-13.7%
Quiet Geomagnetic	0.242	0.283	-14.5%
Moderate Geomagnetic	0.305	0.355	-14.1%

Table 6.3: Cross Correlation Comparison, CHAMP 2009

Bin	Cross Correlation		
	POE Given CD	POE Estimated CD	% Change
Overall	0.955	0.956	-0.105%
Low Solar	0.949	0.950	-0.105%
Moderate Solar	0.940	0.940	0.000%
Quiet Geomagnetic	0.955	0.957	-0.209%
Moderate Geomagnetic	0.951	0.951	0.000%

Table 6.4: RMS Comparison, CHAMP 2009

Bin	Root Mean Square (10^{-12} kg/m^3)		
	POE Given CD	POE Estimated CD	% Change
Overall	0.401	0.461	-13.0%
Low Solar	0.381	0.439	-13.2%
Moderate Solar	0.540	0.618	-12.6%
Quiet Geomagnetic	0.404	0.464	-12.9%
Moderate Geomagnetic	0.332	0.384	-13.5%

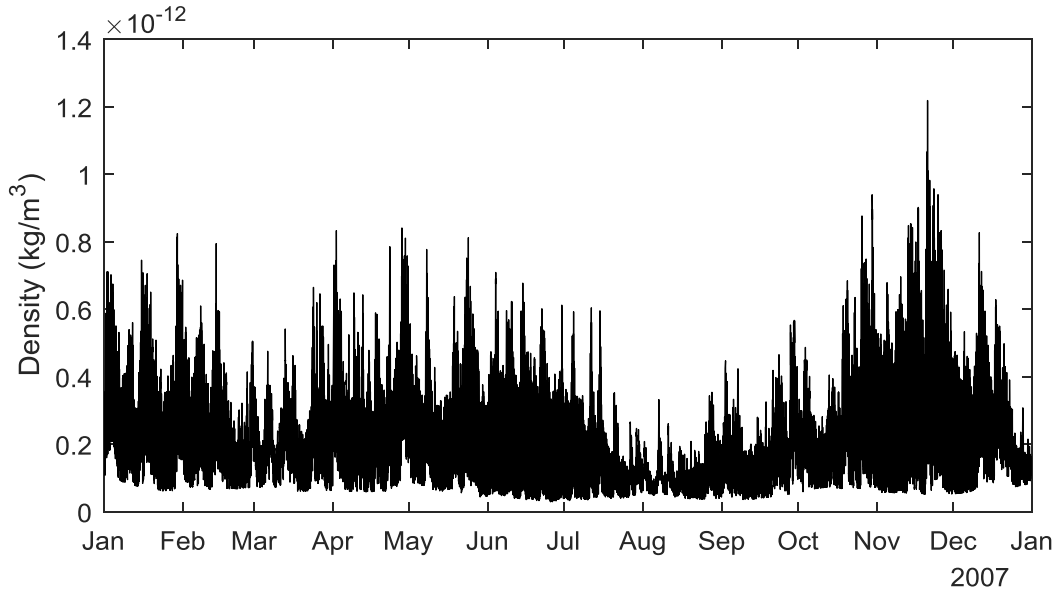

Figure 6.15: GRACE Atmospheric Density Estimates, 2007

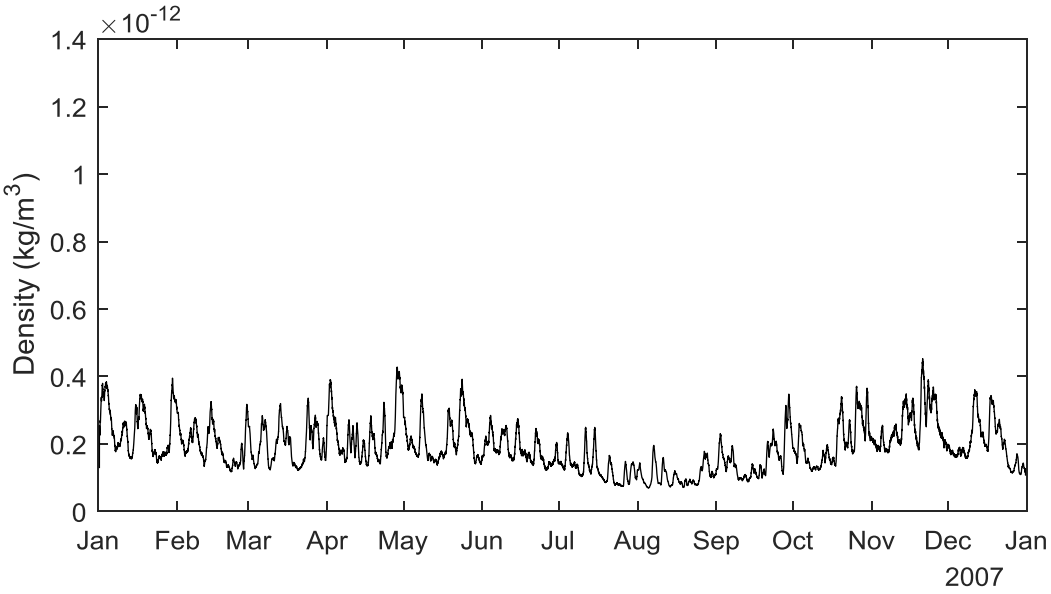

Figure 6.16: GRACE Smoothed Atmospheric Density Estimates, 2007

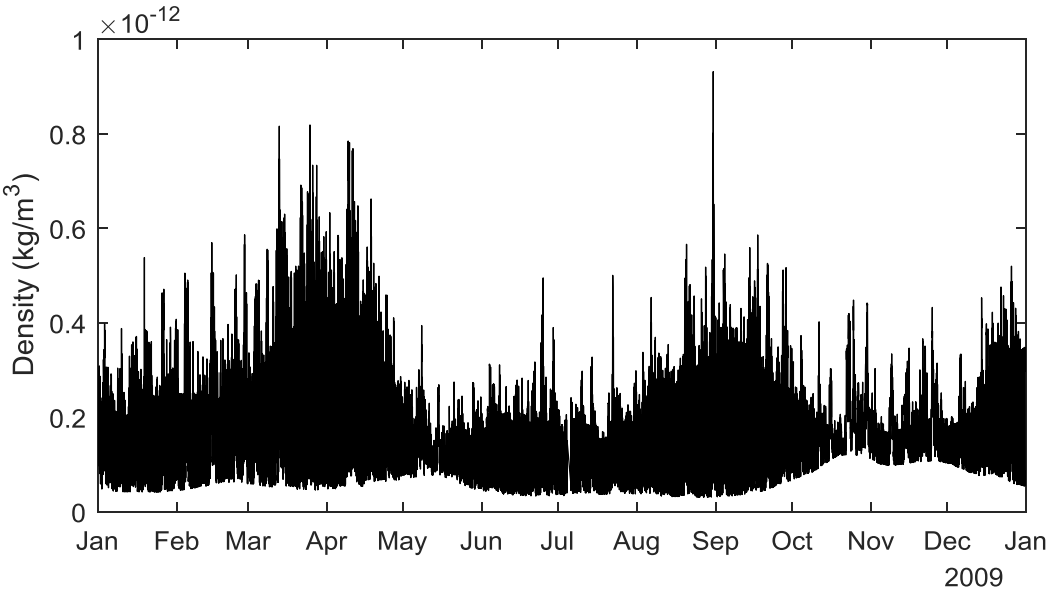

Figure 6.17: GRACE Atmospheric Density Estimates, 2009

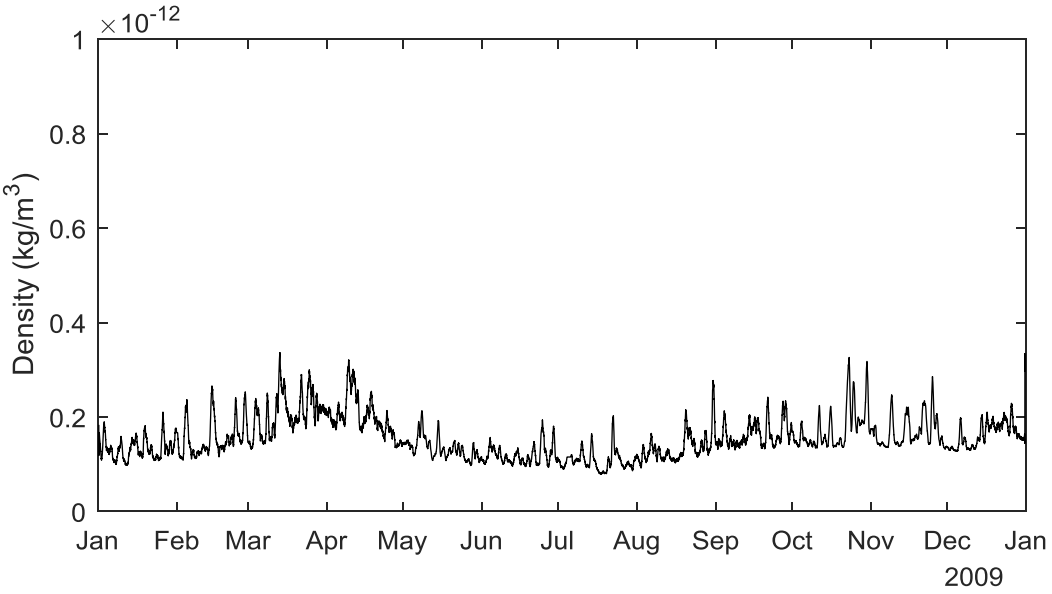

Figure 6.18: GRACE Smoothed Atmospheric Density Estimates, 2009

Table 6.5: Cross Correlation Comparison, GRACE 2007

Bin	Cross Correlation		
	POE Given CD	POE Estimated CD	% Change
Overall	0.912	0.913	-0.110%
Low Solar	0.912	0.912	0.000%
Moderate Solar	0.907	0.910	-0.330%
Quiet Geomagnetic	0.925	0.926	-0.108%
Moderate Geomagnetic	0.883	0.881	0.227%

Table 6.6: RMS Comparison, GRACE 2007

Bin	Root Mean Square (10^{-12} kg/m^3)		
	POE Given CD	POE Estimated CD	% Change
Overall	0.029	0.033	-11.9%
Low Solar	0.028	0.032	-12.6%
Moderate Solar	0.032	0.036	-10.9%
Quiet Geomagnetic	0.025	0.028	-11.4%
Moderate Geomagnetic	0.039	0.045	-12. 7%

Table 6.7: Cross Correlation Comparison, GRACE 2009

Bin	Cross Correlation		
	POE Given CD	POE Estimated CD	% Change
Overall	0.910	0.909	0.110%
Low Solar	0.905	0.899	0.667%
Moderate Solar	0.900	0.910	-1.098%
Quiet Geomagnetic	0.909	0.908	0.110%
Moderate Geomagnetic	0.910	0.916	-0.665%

Table 6.8: RMS Comparison, GRACE 2009

Bin	Root Mean Square (10^{-12} kg/m^3)		
	POE Given CD	POE Estimated CD	% Change
Overall	0.021	0.023	-8.7%
Low Solar	0.020	0.023	-13.0%
Moderate Solar	0.025	0.025	-0.4%
Quiet Geomagnetic	0.021	0.024	-12.7%
Moderate Geomagnetic	0.018	0.020	-10.0%

As seen in Tables 6.1-6.4 above, the introduction of a higher fidelity drag coefficient model resulted in an across the board reduction of the RMS error in the atmospheric density estimates as compared to the accelerometer data. For the CHAMP satellite, the error was reduced by nearly 15% for 2007 and 14% for 2009. The Cross Correlation, however, was also reduced a slight amount compared to the previous results. In these cases, the reduction in cross correlation was very miniscule in comparison to the large reduction in the RMS error. The majority of this reduction in RMS error is attributed to the reduction in bias between the accelerometer density and the POE derived density.

Tables 6.5-6.8 show the same trend for the GRACE mission. For the GRACE satellite in 2007, there was again a major reduction in the RMS values, approximately 11% across the board. For 2009, however, the moderate solar bin only shows a slight reduction in the RMS values. All other bins show a good reduction in RMS however, so this smaller reduction is likely attributed to a small number of values in the bin, and an over performing set of data previously found in this bin. As with the CHAMP satellite, the cross correlation has fluctuated a small amount compared to the original data. However, as before this is a small reduction in most cases, and in some locations, the cross correlation actually increased for the GRACE satellite. Overall, for both satellites, the inclusion of a more accurate drag model has resulted in a quantifiable increase in the accuracy for the atmospheric density estimates.

7 UNCERTAINTY IN ATMOSPHERIC DENSITY ESTIMATES

To validate the results found in the previous section, the uncertainty of the atmospheric density corrections is studied. By examining the scale difference between the RMS errors from accelerometer-derived densities found in the CHAMP and GRACE satellites and the RMS of the uncertainties associated with the estimates, the RMS values for missions without truth-values in the form of accelerometer densities can be estimated.

7.1 Estimation of Scale Factor for Atmospheric Estimate Uncertainty

To help quantify the errors in the estimated atmospheric density for satellites without accelerometer density, the uncertainties in the atmospheric density corrections returned by the smoother are scaled to fit the errors in atmospheric density returned for the CHAMP and GRACE satellites. Figures 7.1 and 7.2 show the error in the estimates compared to the modified Sutton accelerometer derived densities found in Mehta et. al. [15], as well at the uncertainty determined by the smoother for CHAMP in 2007 and 2009 respectively. Figures 7.3 and 7.4 show the same results for the GRACE satellites. Using the scale factor discussed in Section 2.6, uncertainties from the estimates of CHAMP are scaled using the RMS errors from GRACE and compared to the actual RMS error using the accelerometer-derived densities, as shown in Figures 7.5 and 7.6. The process is then repeated for the estimates of GRACE using the results of CHAMP in Figures 7.7 and 7.8.

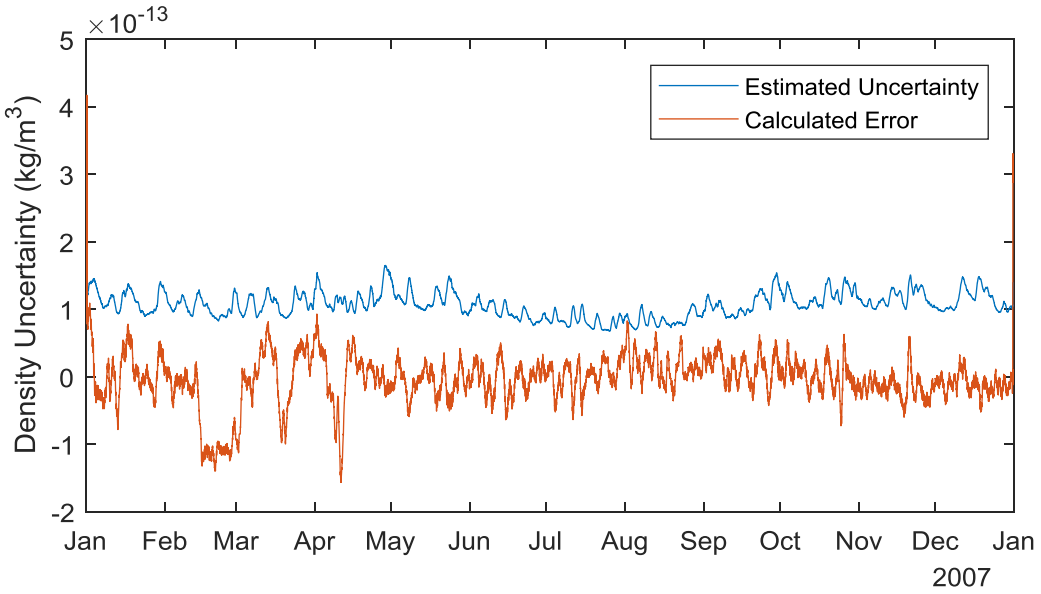

Figure 7.1: CHAMP Estimated Uncertainty Compared to Calculated Error from Accelerometer Derived Density, 2007

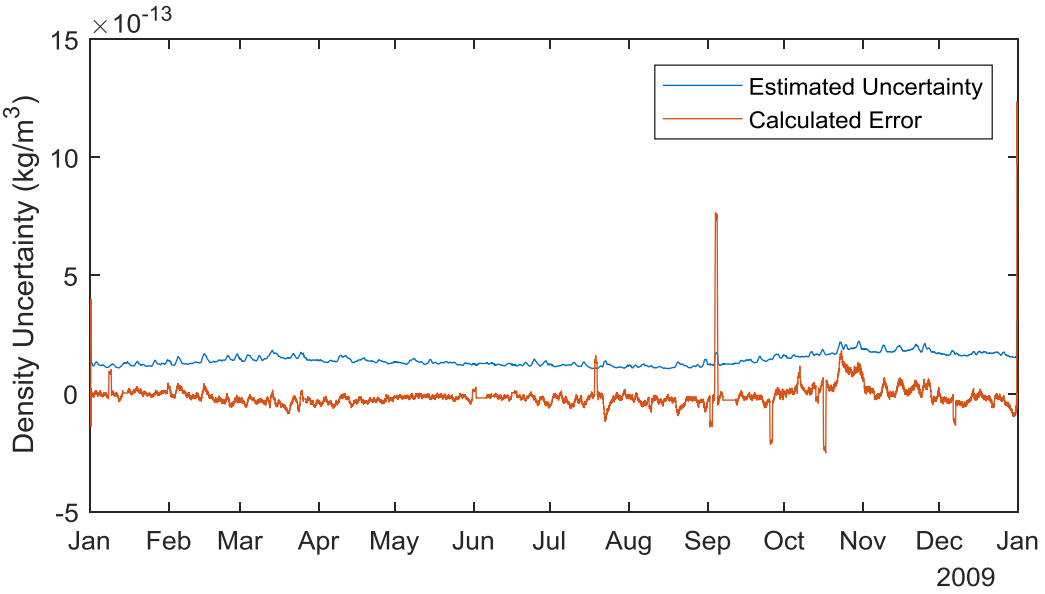

Figure 7.2: CHAMP Estimated Uncertainty Compared to Calculated Error from Accelerometer Derived Density, 2009

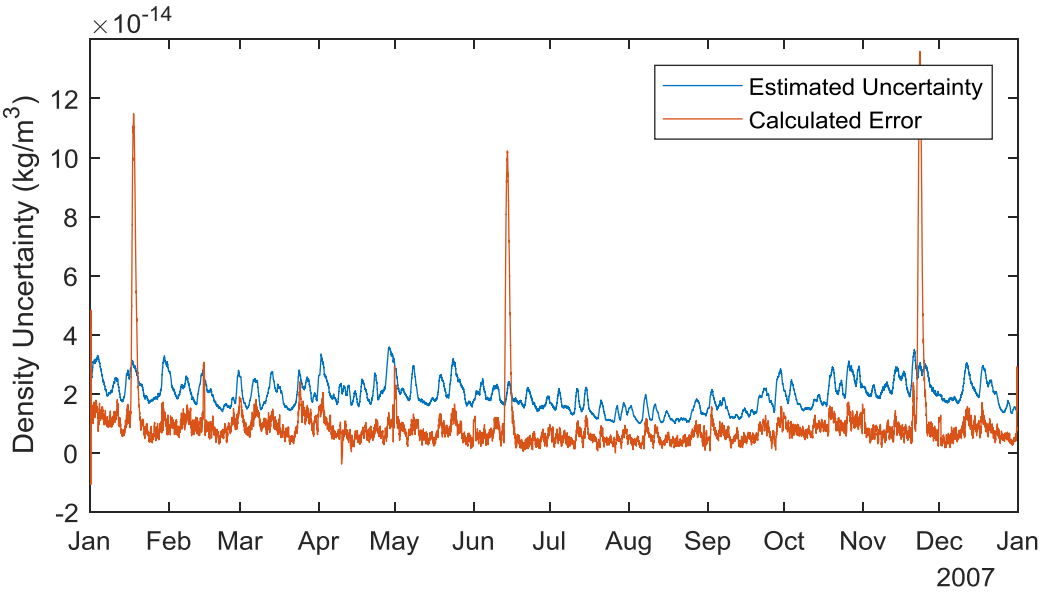

Figure 7.3: GRACE Estimated Uncertainty Compared to Calculated Error from Accelerometer Derived Density, 2007

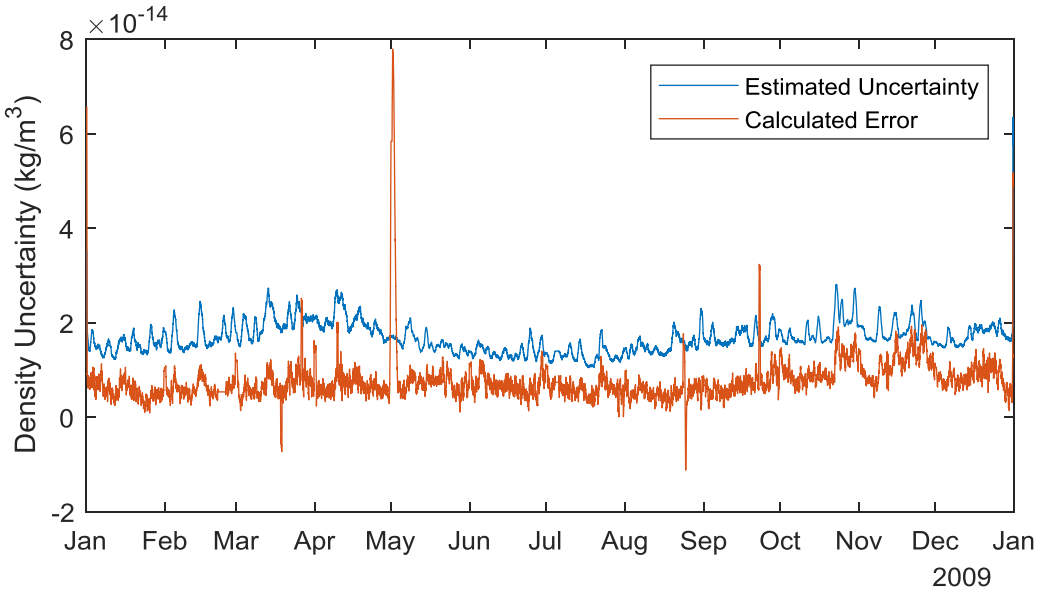

Figure 7.4: GRACE Estimated Uncertainty Compared to Calculated Error from Accelerometer Derived Density, 2009

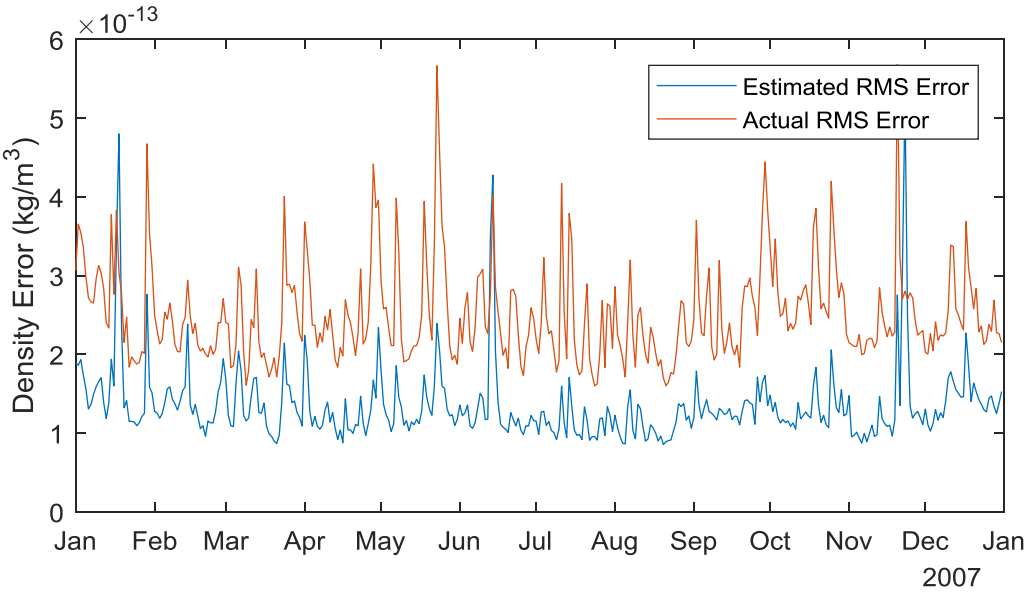

Figure 7.5: CHAMP Actual Daily RMS Errors Compared to Estimated Daily RMS Errors using GRACE Scaling, 2007

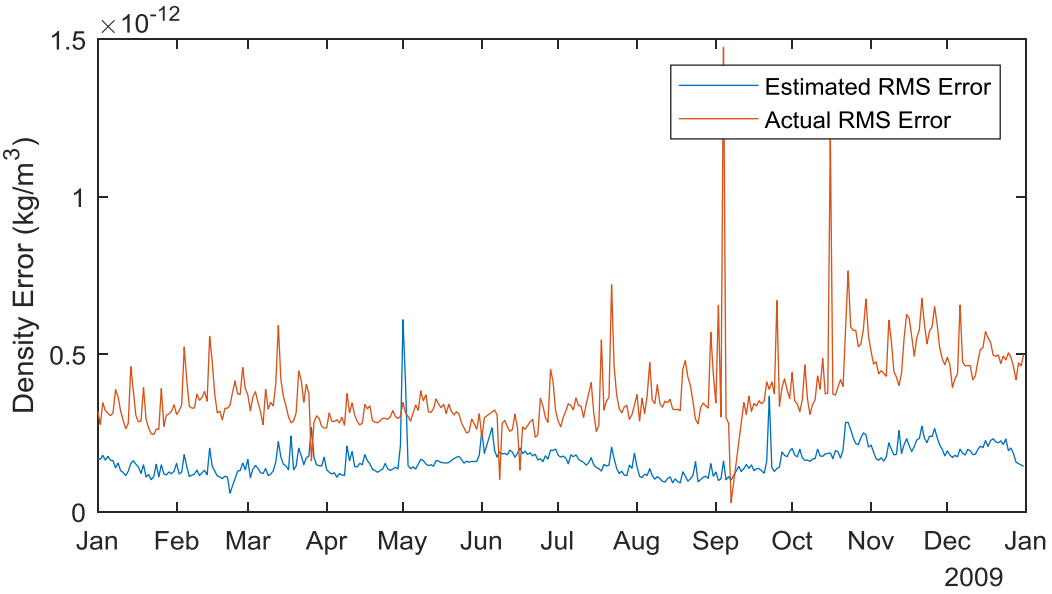

Figure 7.6: CHAMP Actual Daily RMS Errors Compared to Estimated Daily RMS Errors using GRACE Scaling, 2009

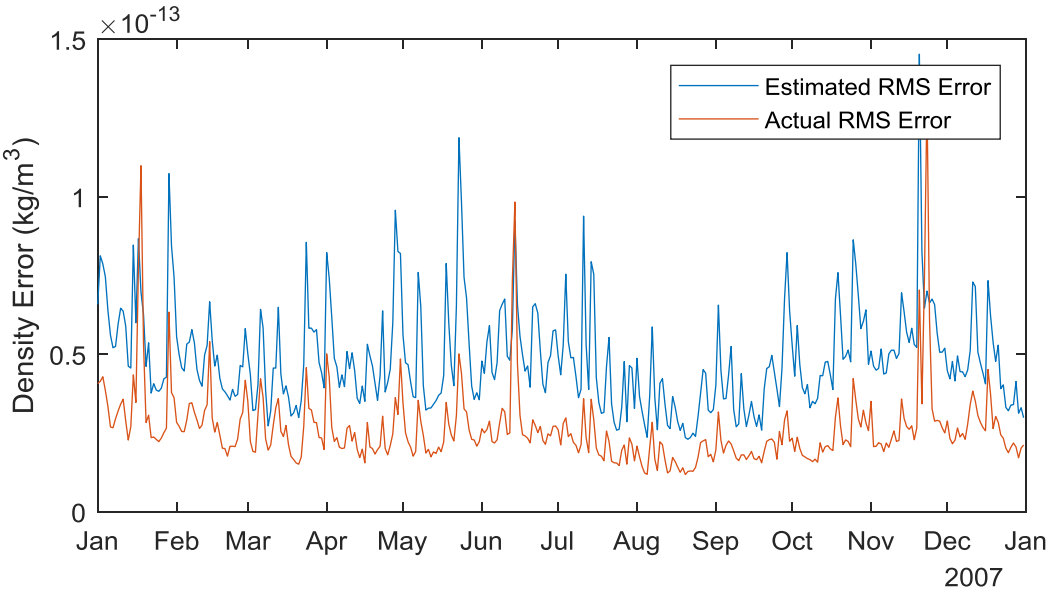

Figure 7.7: GRACE Actual Daily RMS Errors Compared to Estimated Daily RMS Errors using CHAMP Scaling, 2007

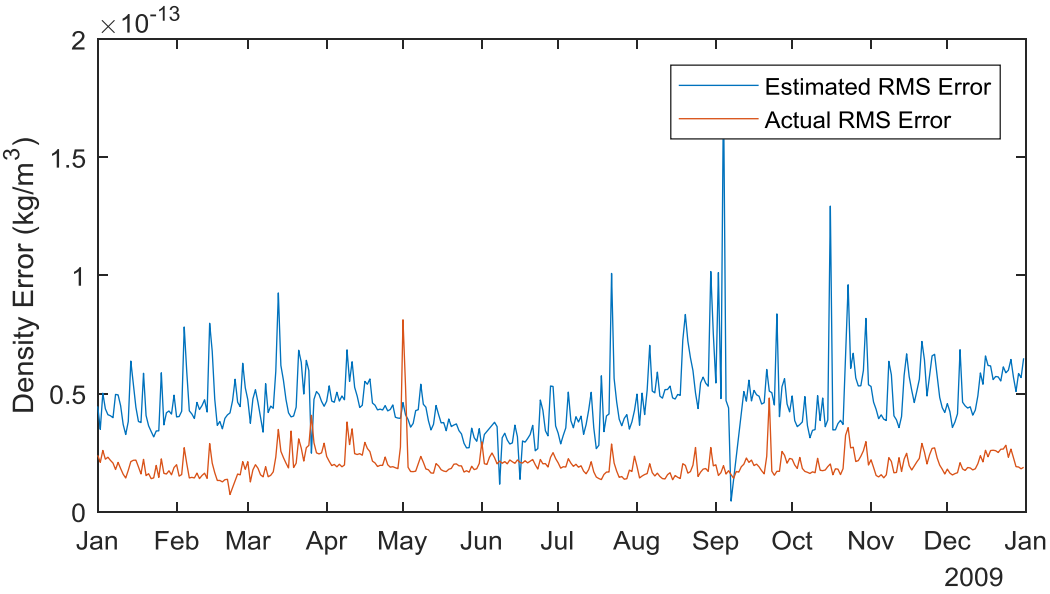

Figure 7.8: GRACE Actual Daily RMS Errors Compared to Estimated Daily RMS Errors using CHAMP Scaling, 2009

As seen in Figures 7.1-7.4, the estimated uncertainty is generally higher than the calculated errors with respect to the accelerometer densities. If the RMS values of the raw uncertainty of the estimates generated by ODTK are used without scaling, these values would provide an overly

conservative estimate of the RMS errors. Through the application of the scaling process, we can reduce the RMS to a more realistic value.

Figures 7.5 and 7.6, which show the CHAMP errors as scaled using the GRACE data, show that applying this scaling has reduced the estimated RMS error too far. The GRACE scaling over-corrects using its scale factor, and therefore is not a suitable candidate to use for scaling the ANDE data, which is closer in altitude to the CHAMP satellite than GRACE. As seen in Figures 7.7 and 7.8 above, using the CHAMP uncertainty scaling provides a conservative estimate of the GRACE errors. This scaling is less conservative, however, than applying the uncertainty measurements directly, and therefore provides a much more realistic result. The CHAMP scaling values will therefore be applied to the ANDE satellites to estimate their RMS error.

7.2 Uncertainty for ANDE Satellites

Using the CHAMP scaling values as determined in Section 7.1, the daily RMS values for the ANDE satellites for the years 2007 and 2009 can be determined using the uncertainty in the estimates. Table 7.1 shows the estimated RMS error for the ANDE-RR MAA satellite using all seven drag coefficient models for 2007 separated into bins as defined in Table 3.1. Tables 7.2 and 7.3 then show the same information for the ANDE-2 satellites Castor and Pollux respectively for the year 2009.

Table 7.1: ANDE-RR MAA Estimated RMS Error Values

	Root Mean Square (10^{-12} kg/m^3)						
	CLL			DRIA			
Bin	Langmuir	Freundlich	Temkin	Langmuir	Freundlich	Temkin	Pilinski
Overall	3.55	3.53	3.53	3.48	3.47	3.48	3.49
Low Solar	3.70	3.68	3.69	3.62	3.61	3.62	3.63
Moderate Solar	3.08	3.08	3.08	3.07	3.08	3.08	3.08
Quiet Geomagnetic	3.49	3.47	3.47	3.41	3.39	3.40	3.42
Moderate Geomagnetic	3.72	3.71	3.71	3.70	3.71	3.71	3.72

Table 7.2: ANDE-2 Castor Estimated RMS Error Values

	Root Mean Square (10^{-12} kg/m^3)						
	CLL			DRIA			
Bin	Langmuir	Freundlich	Temkin	Langmuir	Freundlich	Temkin	Pilinski
Overall	1.54	1.54	1.54	1.54	1.54	1.54	1.54
Low Solar	1.44	1.44	1.44	1.44	1.44	1.44	1.44
Moderate Solar	1.82	1.82	1.82	1.82	1.82	1.82	1.82
Quiet Geomagnetic	1.53	1.53	1.53	1.53	1.53	1.53	1.53
Moderate Geomagnetic	1.79	1.79	1.79	1.79	1.79	1.79	1.79

Table 7.3: ANDE-2 Pollux Estimated RMS Error Values

	Root Mean Square (10^{-12} kg/m^3)						
	CLL			DRIA			
Bin	Langmuir	Freundlich	Temkin	Langmuir	Freundlich	Temkin	Pilinski
Overall	1.64	1.64	1.64	1.64	1.64	1.64	1.64
Low Solar	1.49	1.49	1.49	1.49	1.49	1.49	1.48
Moderate Solar	2.09	2.09	2.09	2.09	2.09	2.09	2.09
Quiet Geomagnetic	1.64	1.64	1.64	1.64	1.64	1.64	1.64
Moderate Geomagnetic	1.76	1.76	1.76	1.76	1.76	1.76	1.77

As seen with the atmospheric density figures found in Section 6.1, the choice of drag coefficient model does not result in a large difference in the results. Each of the respective drag coefficient models appear to provide a similarly accurate estimate of the atmospheric density encountered by the ANDE satellites. The few spikes in the percent difference as seen in Figures 6.3, 6.6, and 6.9 lead to the primary differences in the RMS values as seen in the above tables.

As shown in Table 7.1, the overall lowest estimated RMS value is found by the Freundlich DRIA model. The ANDE-RR MAA results are more representative of the entire lifetime of the satellite, as the entirety of the MAA mission takes place in 2007. Therefore, the differentiation that occurs during re-entry is also captured by the estimates and can be applied to the RMS values. Tables 7.2 and 7.3 do not show much difference in estimated error between the models for the ANDE-2 mission in 2009. Since in neither case, the satellites had dipped low enough in the atmosphere until 2010, the tail end of these missions is not captured. Provided the scaling could be extended into 2010, these models would likely differentiate much like the ANDE-RR MAA satellite and provide a clearer picture of which atmospheric model was most effective.

8 SUMMARY, CONCLUSION, AND FUTURE WORK

8.1 Summary

Precise knowledge of the density in the upper atmosphere is a vital component of the orbit determination process, as inaccuracies in the estimation of atmospheric drag are the primary source of uncertainty for satellites in low Earth orbit. A need for more accurate knowledge of the upper atmosphere, which results in improved accuracy of orbit determination, has led to the development of atmospheric density derived from precision satellite orbits. This method, however, requires more refinement and validation before being put into widespread use. In addition, the uncertainty associated with this POE model prior to the research completed here was not well documented.

To improve these atmospheric density models, the methods of validation for previously completed work were expanded to include the entire lifetime of both the CHAMP and GRACE satellites. These expansions provided a much more robust understanding of the effectiveness of the POE methods over the entire lifetime of these satellites. Additionally, the framework has been set to more easily ingest the results for additional satellite missions to ensure that all data is processed for any future missions.

In some locations, however, there were gaps in the accelerometer derived densities which required an alternative method. By patching together and scaling two separate accelerometer density data sets, a single, more robust data set is provided that allows for a more effective comparison of the estimated POE densities to the truth values.

In an effort to further improve these atmospheric density estimates, results for the spherical ANDE mission satellites were considered in addition to the more complex CHAMP and GRACE

missions. A method of calculating the drag coefficient for a sphere was applied to these missions to allow for a higher fidelity model of the satellite in question. Drag coefficients calculated in a similar method to those used for the ANDE missions and projected area information are also available for the CHAMP and GRACE missions. These values were applied to further improve the estimates of atmospheric density.

Using these drag coefficients, the atmospheric densities were estimated, preserving the uncertainties returned by the filter and smoother for use in further evaluation of the methods. These returned atmospheric densities showed a marked reduction in the RMS values returned for both the CHAMP and GRACE satellites. For the ANDE satellites, however, a method of validation was still required.

This method of validation was developed by examining the results for the CHAMP and GRACE satellites. By comparing the daily RMS values of the uncertainty in the atmospheric density estimates to the daily RMS errors as compared to the accelerometer derived densities, a scale factor for each day is returned. The more conservative estimate is used to estimate the RMS errors for the ANDE satellite missions.

Through the application of these scale factors, a table of RMS values, much like the ones returned for the CHAMP and GRACE satellites in Section 4.2 was generated. These average RMS values, as placed in the respective atmospheric and geomagnetic bins as defined in Table 3.1, provide a first estimate of the accuracy of the atmospheric density estimates for a satellite without any a priori knowledge of the atmospheric density as seen by the satellite. Through this method, the most effective drag coefficient model can be selected.

In conclusion, three distinct advancements have been made.

1. The drag coefficients have been determined for the ANDE satellites using a larger set of methods than have been previously studied, including the CLL method and a series of separate adsorption models.

2. The POE method has been altered to allow for these drag coefficients to be used directly instead of estimated.

3. By investigating the difference in the uncertainties of the CHAMP and GRACE satellites with their RMS errors, the RMS errors for a satellite without a base truth model are provided for the first time.

8.2 Conclusion

Through the work completed in this dissertation the following conclusions are drawn:

1. The POE densities that were previously completed have been successfully re-calculated to ensure no issues with an optimization of code, showing a less than 1% deviation from the originally calculated values found in literature for the provided days.

2. Through the merging of two separate data sets and the examination of CC and RMS values for the entire lifetime of the CHAMP and GRACE satellites, a more thorough and complete understanding of the performance of each metric has been reached.

3. The drag coefficients generated in Section 5 fall within expected values found in literature and are therefore considered to be accurate.

4. The relative differences between the drag coefficients found for the ANDE satellites remained within a 10% envelope for the lifetime of each satellite and under 5% outside of a few locations where the accommodation coefficient fell below the allowable value of 0.85 for the Pilinski derived drag coefficients.

5. The effective area approach to calculating atmospheric density was successful in incorporating the drag coefficients and normal areas into the ODTK filter and smoother techniques.

6. The atmospheric densities calculated for the ANDE series of satellites showed no more than a 10% deviation regardless of drag coefficient model selection, save for a few locations in the ANDE-RR MAA and ANDE-2 Pollux satellites, which showed a large jump in the Langmuir derived models, primarily at the end-of-life for each satellite.

7. The atmospheric densities as calculated for the CHAMP and GRACE satellites provide a more accurate representation of the atmosphere after adding the new drag coefficients and normal areas.

8. By scaling the results from the CHAMP and GRACE missions, an effective value of the root mean square error for satellites without accelerometer derived density truth values can be estimated.

9. Using the RMS values estimated for the ANDE satellites, the Freundlich DRIA model provided the lowest error solution for the ANDE-MAA satellite and was the second lowest error model next to the Pilinski values for the ANDE-2 missions.

8.3 Future Work

Through the work completed in this research, additional tasks have arisen which merit further study. Some suggested topics of future study are listed in this section.

8.3.1 Drag Coefficient Resolution Cost-Benefit Analysis

In completing the estimation of the atmospheric densities, the values for drag coefficient on a minute-by-minute basis were imported into the model to ensure a high accuracy solution. However, this process can be computationally expensive, both in the generation of the drag coefficients and the ingesting of them into the orbit determination process. One avenue of research to be studied is the reduction of the resolution of the input drag coefficients. While a brief investigation has been performed in Section 6.1, the one day averaging was too severe. A cost-benefit analysis of the computing time used to generate the drag coefficients compared to the benefit of the higher fidelity in the atmospheric density estimation could provide a more efficient solution.

8.3.2 Examination of Effectiveness of Scaling Process on Other Known Satellites

To further evaluate the effectiveness of the scaling process, additional satellite missions with overlapping data should be explored to determine the effectiveness of this method. Adding more data points at different altitudes and atmospheric conditions will help to provide a more robust understanding of the scaling process.

8.3.3 **Generalization of Scaling Process**

The scaling process as presented in Section 7 is limited to areas in which a precursor satellite with an established accelerometer density is able to calculate the error and the scale factor for a set day. Realistically, a more generalized solution would be necessary to expand this method into areas where no precursor satellite is available. Using the CHAMP and GRACE missions, in accordance with a few additional missions to provide more data points, the scale factors may be distilled down to something that can be estimated using a set of inputs.

REFERENCES

1. Vallado, D. A. *Fundamentals of Astrodynamics and Applications*. Hawthorne, CA: Microcosm Press, 2013.
2. McLaughlin, C. A., Hiatt, A., and Lechtenberg, T. "Precision Orbit Derived Total Density," *Journal of Spacecraft and Rockets* Vol. 48, No. 1, 2011, pp. 166-174. doi: 10.2514/1.47624
3. McLaughlin, C. A., Godinez, H., and Sizemore, A. "The Effects of Assimilating Various Data into General Circulation Models on Model Output Density," *AGU Fall Meeting Abstracts*. 2017.
4. Wright, J. R. "Real-time estimation of local atmospheric density," *Advances in the Astronautical Sciences* Vol. 114, 2003, pp. 927-950.
5. Wright, J. R. "Simultaneous real-time estimation of atmospheric density and ballistic coefficient," *Advances in the Astronautical Sciences* Vol. 119, 2004, pp. 1155-1184.
6. Jacchia, L. G. "Revised Static Models of the Thermosphere and Exosphere with Empirical Temperature Profiles." Cambridge, MA, 1971.
7. Roberts, C. E. "An analytic model for upper atmosphere densities based upon Jacchia's 1970 models," *Celestial mechanics* Vol. 4, No. 3, 1971, pp. 368-377. doi: 10.1007/bf01231398
8. Bowman, B. R., Tobiska, W. K., Marcos, F. A., Huang, C. Y., Lin, C. S., and Burke, W. J. "A new empirical thermospheric density model JB2008 using new solar and geomagnetic indices," *AIAA/AAS Astrodynamics Specialist Conference, AIAA*. Vol. 6438, 2008, p. 2008.
9. Stickland, A. "CIRA 1972: COSPAR international reference atmosphere 1972," *Berlin, East Germany, Akademie-Verlag GmbH, 1972. 460 p*, 1972.
10. Hedin, A. E. "Extension of the MSIS thermosphere model into the middle and lower atmosphere," *Journal of Geophysical Research: Space Physics* Vol. 96, No. A2, 1991, pp. 1159-1172.
11. Picone, J. M., Hedin, A. E., Drob, D. P., and Aikin, A. C. "NRLMSISE-00 empirical model of the atmosphere: Statistical comparisons and scientific issues," *Journal of Geophysical Research: Space Physics* Vol. 107, No. A12, 2002, pp. SIA 15-1-SIA 15-16. doi: 10.1029/2002JA009430
12. Mysore Krishna, D. "Improving and Expanding Precision Orbit Derived Atmospheric Densities," *Aerospace Engineering*. Vol. MS, University of Kansas, 2012, p. 203.
13. Sutton, E. K. "Accelerometer-Derived Atmospheric Density from the CHAMP and GRACE Satellites." Air Force Research Laboratory (AFRL/RVBX), 2011.
14. Bruinsma, S., and Biancale, R. "Total Densities Derived from Accelerometer Data," *Journal of Spacecraft and Rockets* Vol. 40, No. 2, 2003, pp. 230-236. doi: 10.2514/2.3937

15. Mehta, P. M., Walker, A. C., Sutton, E. K., and Godinez, H. C. "New density estimates derived using accelerometers on board the CHAMP and GRACE satellites," *Space Weather* Vol. 15, No. 4, 2017, pp. 558-576.
doi: 10.1002/2016SW001562
16. McLaughlin, C. A., Lechtenberg, T., Fattig, E., and Mysore Krishna, D. "Estimating Density Using Precision Satellite Orbits from Multiple Satellites," *The Journal of the Astronautical Sciences* Vol. 59, No. 1, 2012, pp. 84-100.
doi: 10.1007/s40295-013-0007-4
17. Mehta, P. M., Walker, A., McLaughlin, C. A., and Koller, J. "Comparing Physical Drag Coefficients Computed Using Different Gas–Surface Interaction Models," *Journal of Spacecraft and Rockets* Vol. 51, No. 3, 2014, pp. 873-883.
doi: 10.2514/1.A32566
18. Moe, M. M., Wallace, S. D., and Moe, K. "Recommended drag coefficients for aeronomic satellites," *The Upper Mesosphere and Lower Thermosphere: A Review of Experiment and Theory, Geophys. Monogr. Ser* Vol. 87, 1995, pp. 349-356.
19. Moe, K., Moe, M. M., and Wallace, S. D. "Drag coefficients of spheres in free-molecular flow," *Advances in the Astronautical Sciences* Vol. 93, 1996, pp. 391-406.
20. Pilinski, M. D., Argrow, B. M., and Palo, S. E. "Semiempirical Model for Satellite Energy-Accommodation Coefficients," *Journal of Spacecraft and Rockets* Vol. 47, No. 6, 2010, pp. 951-956.
doi: 10.2514/1.49330
21. Bowman, B. R., and Moe, K. "Drag coefficient variability at 175-500 km from the orbit decay analyses of spheres," *Paper AAS 05-257 presented at the AIAA/AAS Astrodynamics Specialist Conference. Lake Tahoe, California*. 2005.
22. Langmuir, I. "The adsorption of gases on plane surfaces of glass, mica and platinum," *Journal of the American Chemical society* Vol. 40, No. 9, 1918, pp. 1361-1403.
23. Cercignani, C., and Lampis, M. "Kinetic models for gas-surface interactions," *Transport Theory and Statistical Physics* Vol. 1, No. 2, 1971, pp. 101-114.
doi: 10.1080/00411457108231440
24. Walker, A., Mehta, P., and Koller, J. "Drag Coefficient Model Using the Cercignani–Lampis–Lord Gas–Surface Interaction Model," *Journal of Spacecraft and Rockets* Vol. 51, No. 5, 2014, pp. 1544-1563.
doi: 10.2514/1.A32677
25. Freundlich, H. *Kapillarchemie: eine Darstellung der Chemie der Kolloide und verwandter Gebiete*: akademische Verlagsgesellschaft, 1922.
26. Walker, A. C., Mehta, P., and Koller, J. "The effect of different adsorption models on satellite drag coefficients," *Advances in the Astronautical Sciences*. Vol. 150, Univelt Inc., 2013, pp. 675-686.

27. Kramer, H. J., "CHAMP (Challenging Minisatellite Payload)," Last Accessed: November 15, 2017, https://directory.eoportal.org/web/eoportal/satellite-missions/c-missions/champ
28. Kramer, H. J., "GRACE (Gravity Recovery And Climate Experiment)," Last Accessed: November 15, 2017, https://directory.eoportal.org/web/eoportal/satellite-missions/g/grace
29. Nicholas, A., Thonnard, S., and Galysh, I. "An Overview Of The ANDE Risk Reduction Flight," *Proceedings of the AMOS Technical Conference*. Maui, HI, 2002.
30. Nicholas, A., Picone, J., Emmert, J., DeYoung, J., Healy, L., Wasiczko, L., Davis, M., and Cox, C. "Preliminary results from the atmospheric neutral density experiment risk reduction mission," *Proc. of the AAS/AIAA Astrodynamics Specialist Conference, paper# AAS*. 2007, pp. 07-265.
31. Kramer, H. J., "ANDE (Atmospheric Neutral Density Experiment)," Last Accessed: August 24, 2018, https://directory.eoportal.org/web/eoportal/satellite-missions/a/ande
32. Kramer, H. J., "ANDE-2 (Atmospheric Neutral Density Experiment-2)," Last Accessed: November 15, 2017, https://directory.eoportal.org/web/eoportal/satellite-missions/a/ande-2
33. Nicholas, A. C., Finne, T., Davis, M. A., and Kessel, R. "Atmospheric Neutral Density Experiment (ANDE-2) Flight Hardware Details." Citeseer, 2009.
34. Storz, M. F., Bowman, B. R., Branson, M. J. I., Casali, S. J., and Tobiska, W. K. "High accuracy satellite drag model (HASDM)," *Advances in Space Research* Vol. 36, No. 12, 2005, pp. 2497-2505.
doi: https://doi.org/10.1016/j.asr.2004.02.020
35. Holmes, S., "RMS Error," Last Accessed: 8/27/2018, http://statweb.stanford.edu/~susan/courses/s60/split/node60.html
36. Bourke, P., "Cross Correlation," Last Accessed: 8/27/2018, http://paulbourke.net/miscellaneous/correlate/
37. de Myttenaere, A., Golden, B., Le Grand, B., and Rossi, F. "Mean Absolute Percentage Error for regression models," *Neurocomputing* Vol. 192, 2016, pp. 38-48.
doi: https://doi.org/10.1016/j.neucom.2015.12.114
38. Goodman, F. O., and Wachman, H. Y. "Formula for thermal accommodation coefficients," *The Journal of Chemical Physics* Vol. 46, No. 6, 1967, pp. 2376-2386.
39. Laurendeau, N. M. *Statistical Thermodynamics: Fundamentals and Applications*: Cambridge University Press, 2005.
40. McLaughlin, C. A., T. F. Lechtenberg, S. Shelton, and A.Sizemore. "Precision Orbit Derived Atmospheric Density: An Update," *Advances in the Astronautical Sciences, 2015* Vol. 155, 2015, pp. 2747-2760.